Sex-specific Genetic Regulatory Effects in Chickens

The supplementary information contains:

Supplementary Figures

Supplementary Tables

Supplementary Data

List of Supplementary Figures:

List of Supplementary Tables:

List of Supplementary Data (in a separate file)**:**

Data S1. Information of 8,265 bulk RNA-seq samples across 32 tissues from 280 ChickenSexGTEx cohort

Data S2. Metadata of 280 ChickenSexGTEx individuals

Data S3. Variance of gene expression explained by recorded metadata

Data S4. Marker gene lists used to annotate 127 different cell types across 31 tissues

Data S5. Cell fractions deconvoluted from 7,969 bulk RNA-seq samples.

Data S6. Summary of genes with sex-biased expression across 30 tissues

Data S7. Summary of sex-biased gene expression networks across 30 tissues

Data S8. Summary of sex-biased cell types across 30 tissues

Data S9. Summary of sex-biased eQTL across 30 chicken tissues

Data S10. Mediation analysis of sex-biased eQTL by TF expression, cell fraction, and gene expression network module.

Data S11. Fine mapping results of leading SV across 32 tissues

Data S12. Summary of significant loci identified from serum lipid metabolite GWAS

Data S13. Summary of sex-different serum lipid GWAS loci explained by sex-biased regulatory variants

Data S14. LDSC enrichement of chicken sQTL on genetic architectures of human complex traits

Data S15. Summary statistics of GWAS results from human complex traits

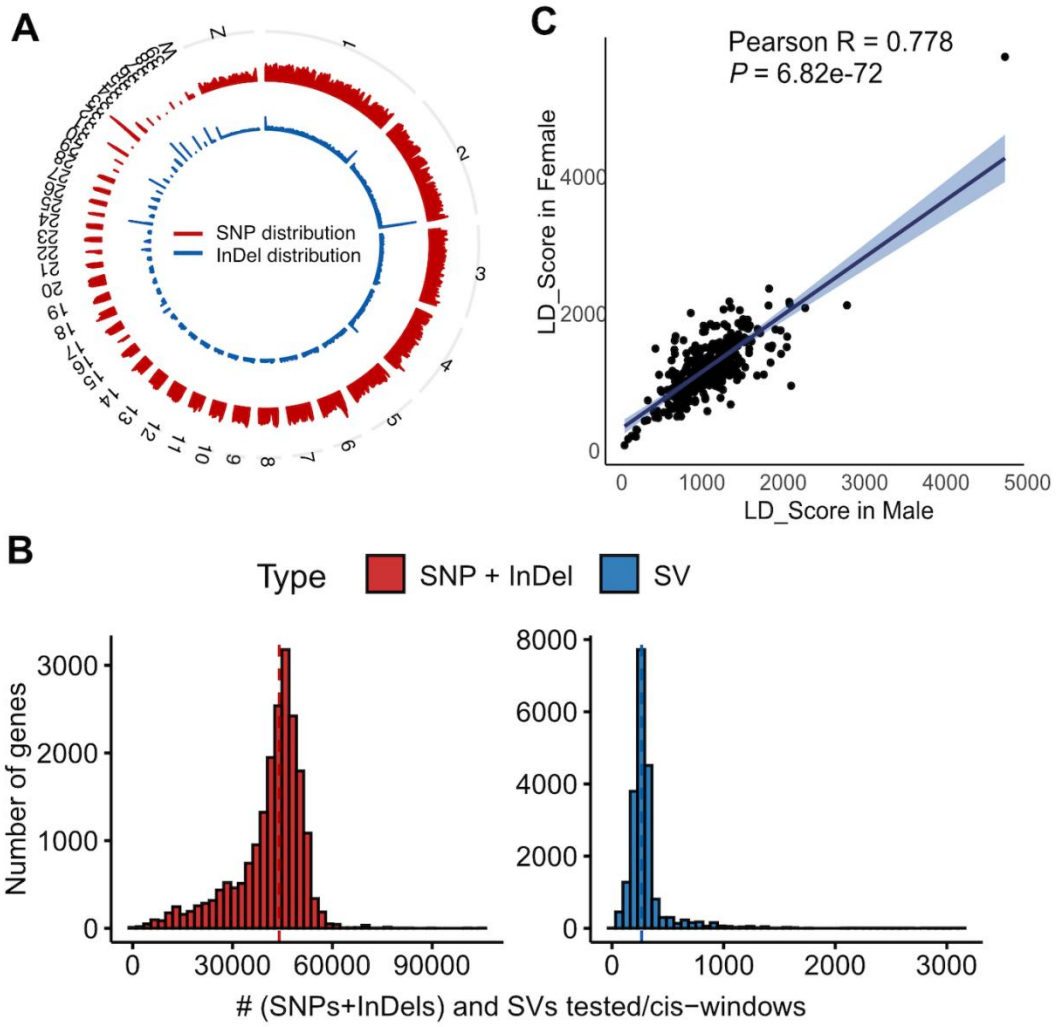

Supplementary Fig. 1. Genotypic characteristics of the ChickenSexGTEx cohort
(A) Genome-wide density distribution of single-nucleotide polymorphism (SNP) and insertion/deletion (InDel) across the chicken genome. Densities were calculated as the number of variants per 1MB. **(B)** Count of genetic variants within ±1 Mb flanking the transcription start site (TSS) of target genes. Left y-axis (red): counts of SNP and InDel. Right y-axis (blue): counts of SVs. **(C)** Linkage disequilibrium (LD) score distribution of SNPs genotyped in male- and female-stratified subpopulations. LD is measured as Pearson r^2. Solid lines represent the smoothed average LD decay, with shaded areas indicating the 95% confidence interval.

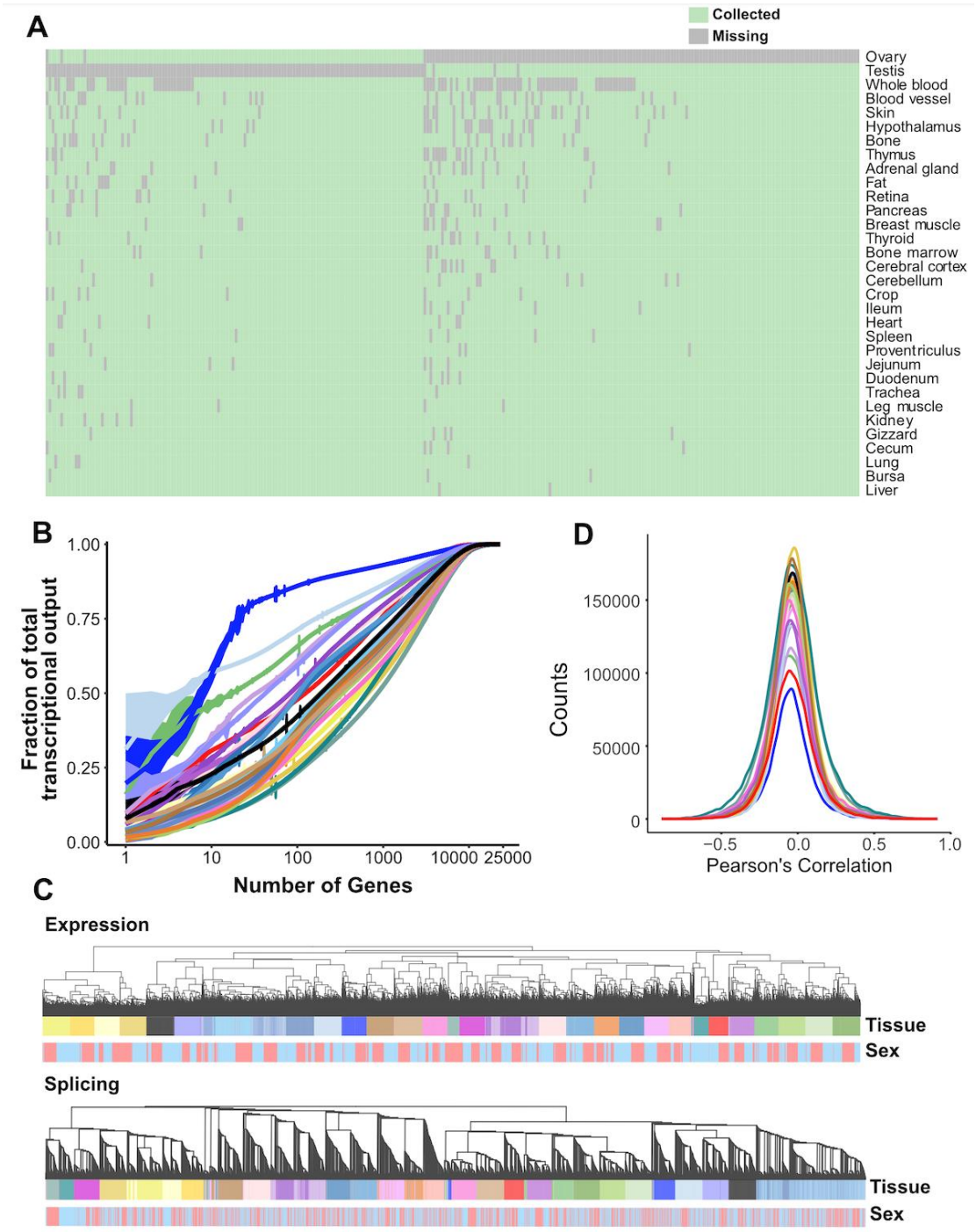

Supplementary Fig. 2. Tissue sample collection and transcriptomic profiling of the ChickenSexGTEx cohort

(A) Matrix of successfully collected tissue samples from 280 individuals. Columns represent individual chickens, and rows represent tissue types. Green blocks indicate collected samples; gray indicates missing samples. **(B)** Cumulative fraction of normalized total expression (sum of TPM) is plotted against the number of detected genes per tissue (TPM ≥ 1). Tissue types are color-coded, consistent with the color key provided in Fig. 2E. **(C)** Hierarchical clustering of samples based on gene expression (top panel) and alternative splicing patterns (bottom panel).

Clustering is generated using the top 5,000 most variably expressed genes or splicing events (measured by coefficient of variation). Tissue and sex categories follow the color key in Fig. 2E. **(D)** Pairwise Pearson's correlation matrices across tissues for gene expression and alternative splicing profiles. Tissue types are color-coded as specified in Fig. 2E.

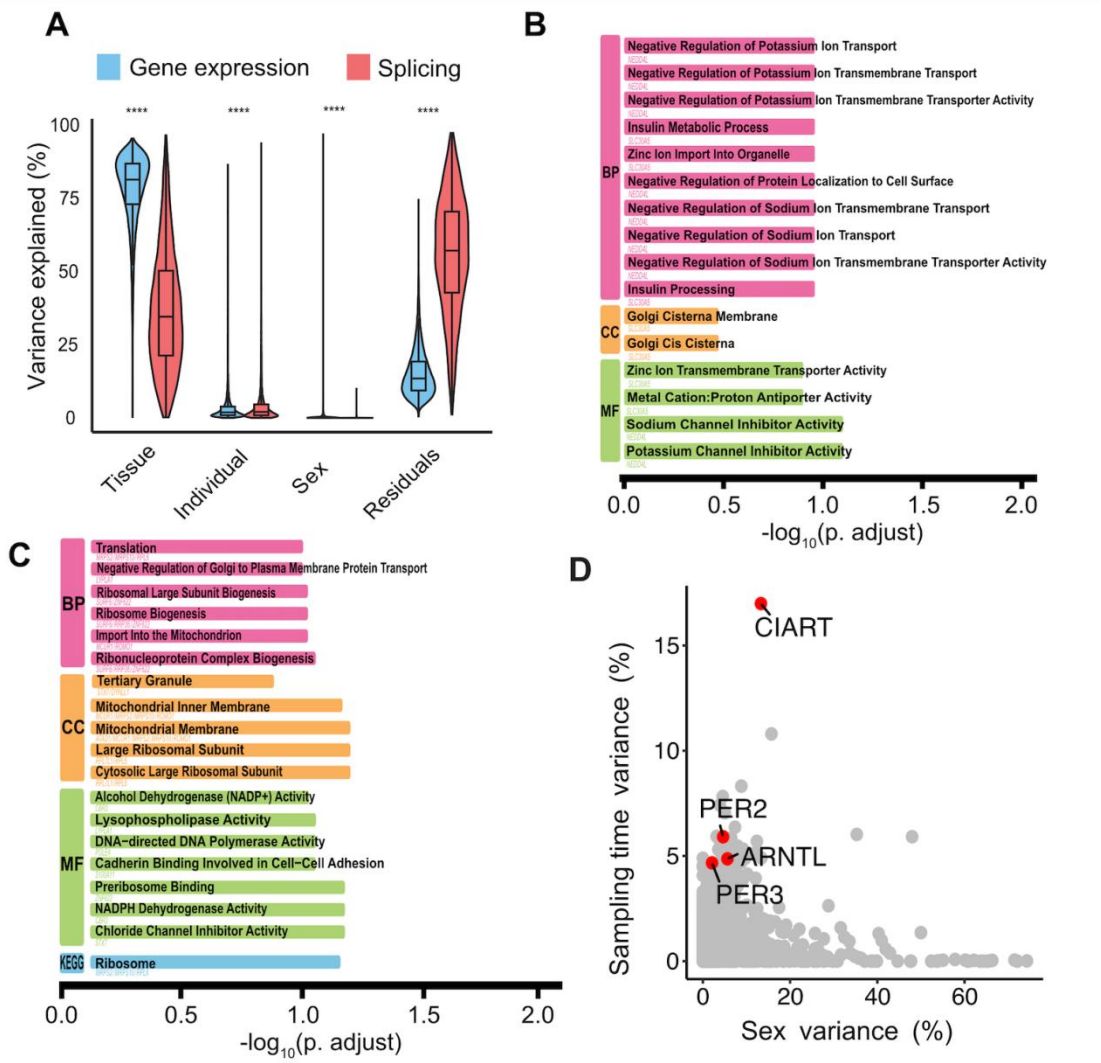

Supplementary Fig. 3. Partitioning of variance in gene expression and alternative splicing, and functional enrichment

(A) Proportion of variance in gene expression and alternative splicing explained by tissue, individual, and sex. **(B)** Gene Ontology (GO) and Kyoto Encyclopedia of Genes and Genomes (KEGG) enrichment results for genes whose expression variance is predominantly driven by sex. **(C)** GO and KEGG enrichment results of genes whose alternative splicing variance is mainly driven by individual-specific effects. **(D)** Partitioning of variance in gene expression attributed to sampling time and sex, quantified by analysis of variance (ANOVA). Each point represents one gene, plotted by variance explained by sex (x-axis) versus sampling time (y-axis). Genes associated with circadian rhythm are highlighted in red.

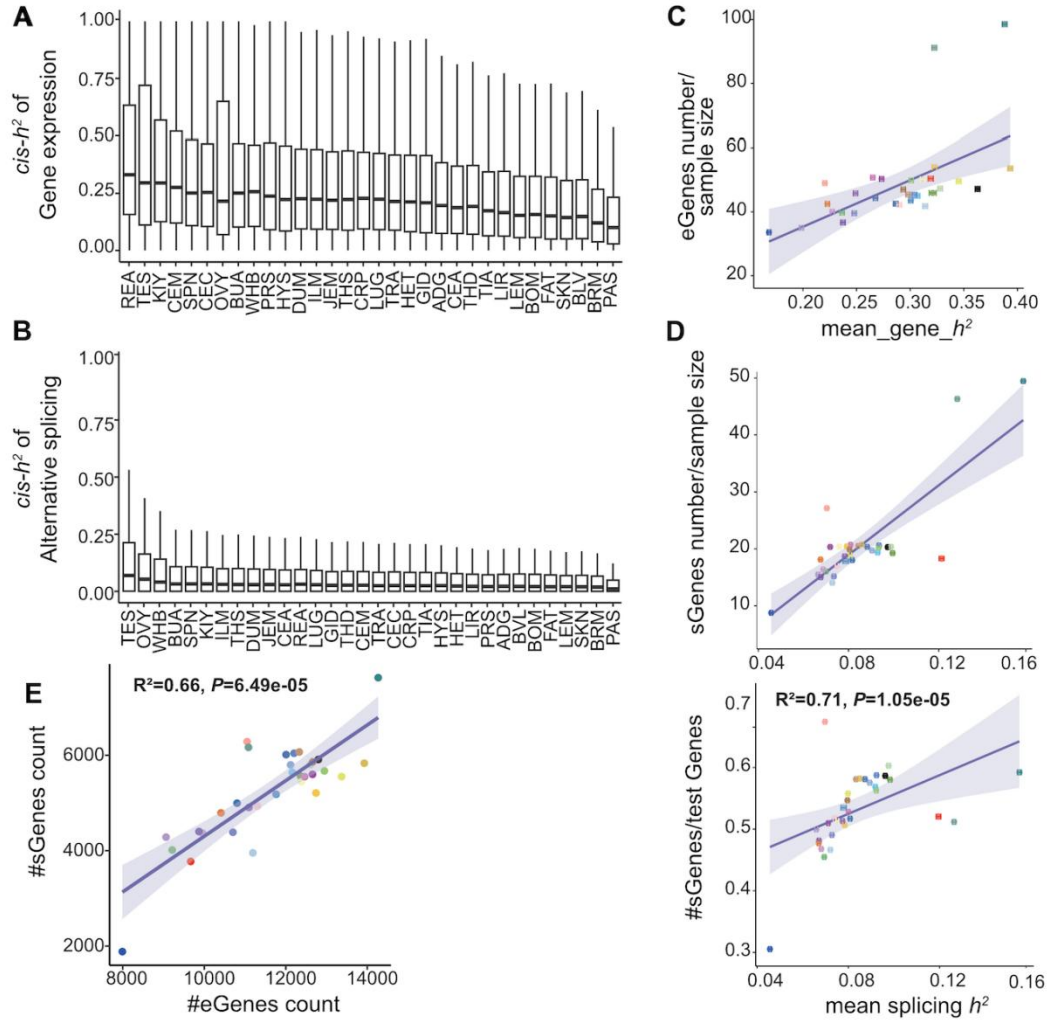

Supplementary Fig. 4. *cis*-h^2 of gene expression and alternative splicing, and impacts on e/sGene detection

(A) *cis*-h^2 estimates of gene expression across 32 tissues. **(B)** *cis*-h^2 estimates of alternative splicing across 32 tissues. **(C)** Correlation between the average *cis*-h^2 of gene expression and the number of eGenes per sample size. **(D)** Correlation between the average *cis*-h^2 of gene alternative splicing and the number of sGenes per sample size (top) and per tested gene set (bottom), respectively. **(E)** Correlation between the number of eGenes and sGenes across 32 tissues.

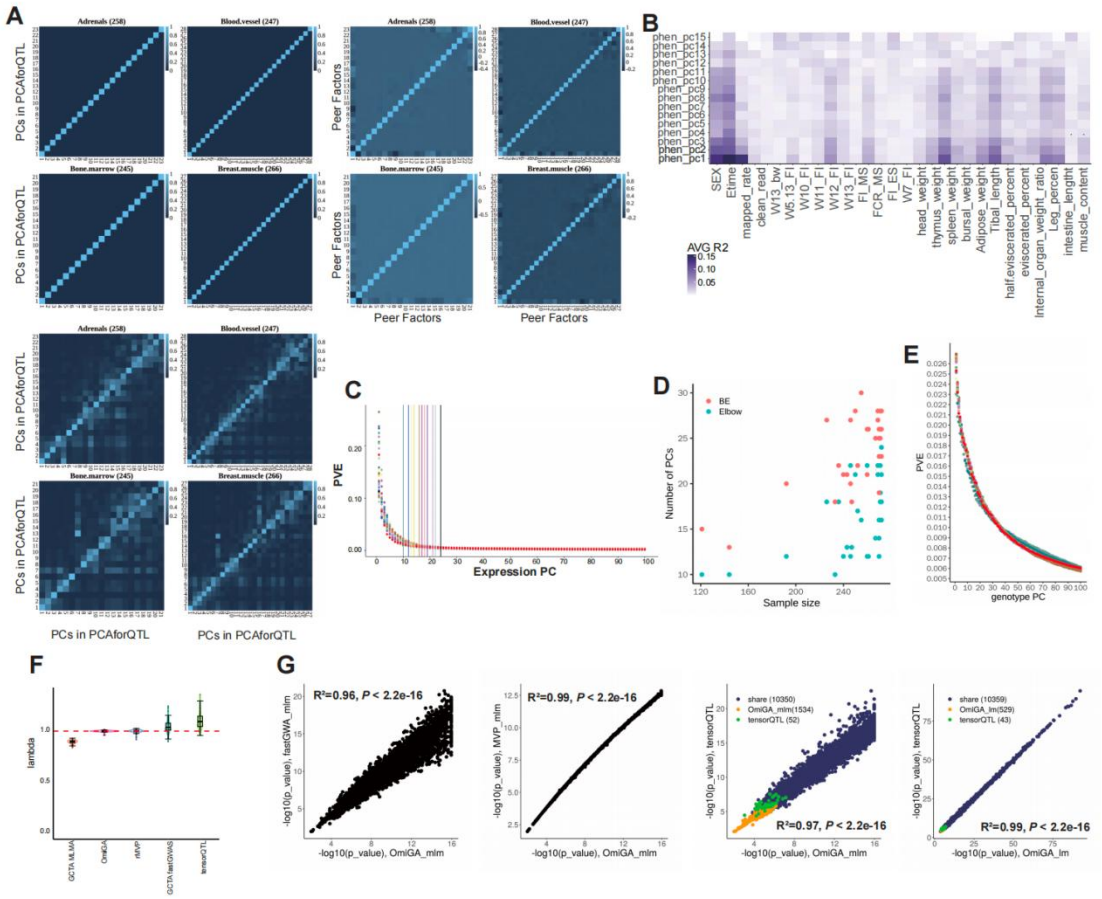

Supplementary Fig. 5. *cis*-molQTL mapping modeling
(A) Correlation of predicted covariates for gene expression, derived from PCAforQTL and PEER factor analysis in representative tissues. **(B)** Average correlation between the top 15 predicted covariates per tissue and recorded experimental metadata. **(C)** Proportion of variance explained (PVE) by ordered principle components (PCs) of gene expression. Lines denote elbow points for optimal PC selection. Tissue types are color-coded as specified in Fig. 2E. **(D)** Number of expression PCs selected via two different methods across 32 tissues. **(E)** PVE by ordered PCs of genotype data. Tissue types are color-coded as specified in Fig. 2E. **(F)** Comparison of genomic inflation control efficiency across linear model approaches: GCTA_MLMA, OmiGA, rMVP_mlm, and GCTA_fastGWA (linear mixed models) versus tensorQTL (general linear model). **(G)** Comparison of the statistical power of linear model and linear mixed model to detect cis-eQTL in liver tissue.

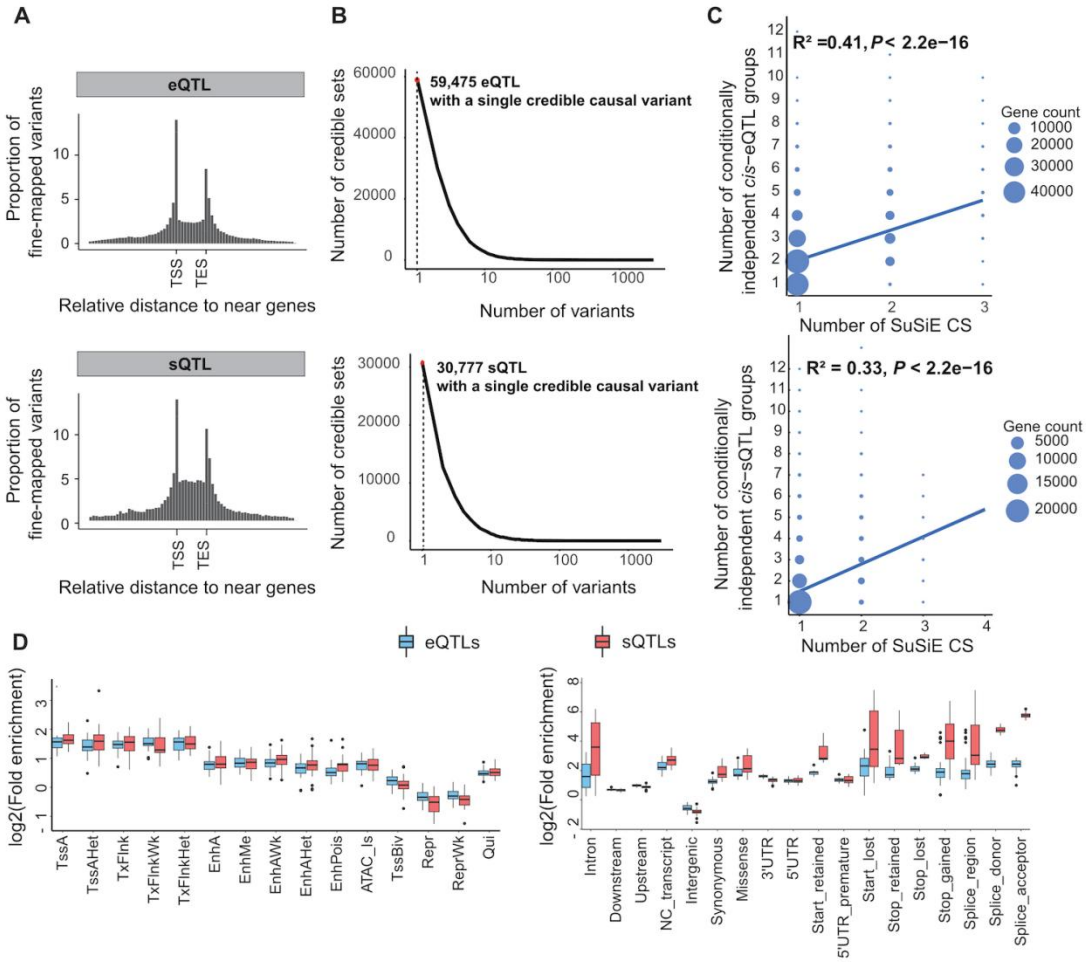

Supplementary Fig. 6. Fine-mapping of *cis*-molQTL and functional annotation
(A) Proportion of fine-mapped eQTL and sQTL plotted against their distance to the TSS and TES of target genes. **(B)** Number of variants in 95% fine-mapped credible sets of eQTL (top) and sQTL (bottom), respectively. **(C)** Correlation between the number of fine-mapped credible sets and the number of conditionally independent molQTL. The top panel shows results for eQTL; the bottom one shows results for sQTL. **(D)** Enrichment analysis of eQTL and sQTL in annotated functional elements (left panel) and genomic regions (right panel) across the chicken genome.

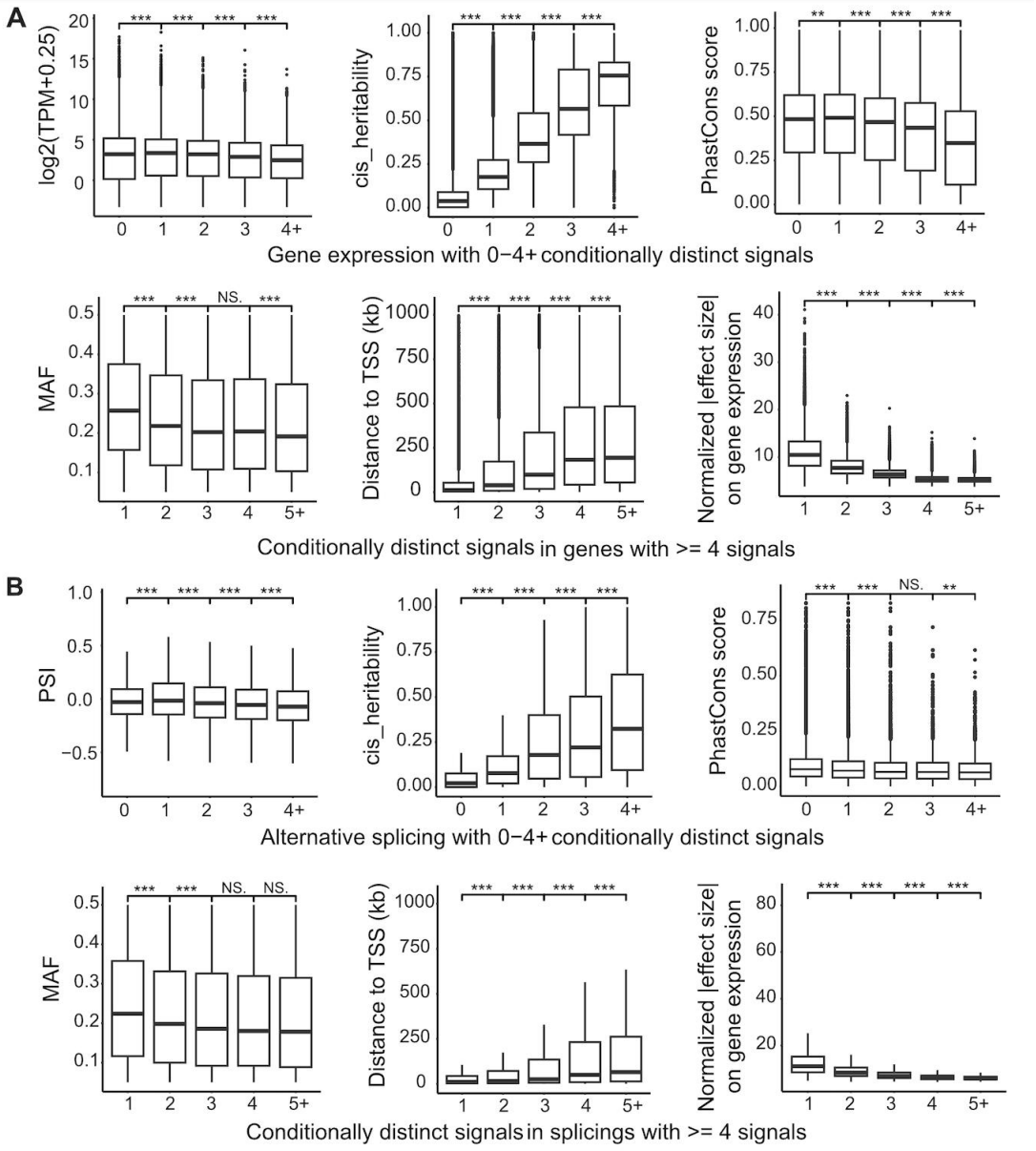

Supplementary Fig. 7. Characterization of allelic heterozygosity in eGenes and sGenes
(A) Boxplots showing gene expression levels, *cis*-h^2, and genome conservation scores for genes regulated by 0–4 independent eQTL (top three panels); and minor allele frequency (MAF), distance to TSS, and effect size for eQTL stratified by significance rank (bottom three panels). **(B)** Boxplots showing alternative splicing event abundance, *cis*-h^2, and genome conservation scores for genes regulated by 0–4 independent sQTL (top three panels); and MAF, distance to TSS, and effect size for sQTL stratified by significance rank (bottom three panels).

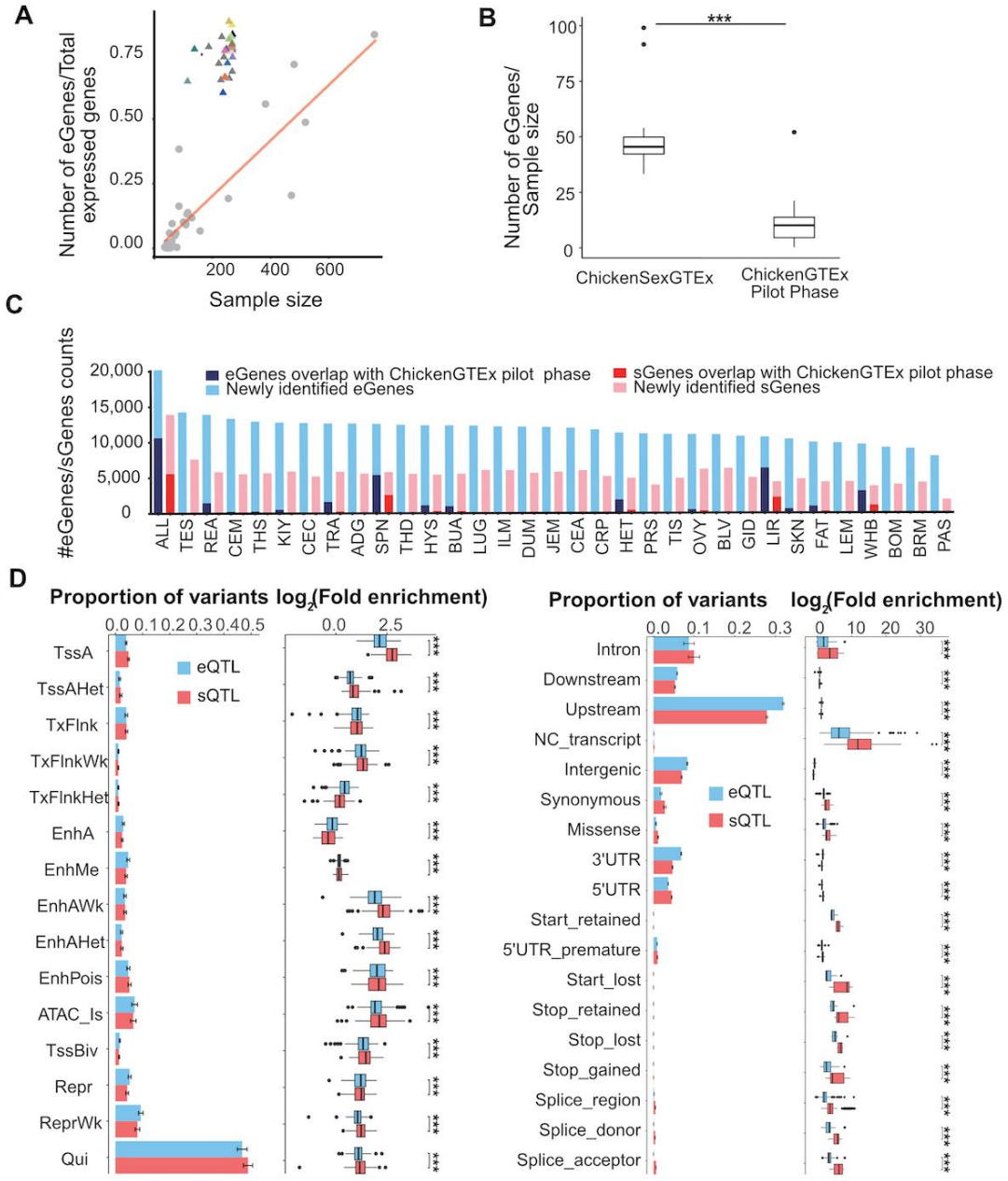

Supplementary Fig. 8. Comparative analysis of eGene/sGene detection power across studies **(A)** Number of eGenes per expressed gene detected in the ChickenSexGTEx cohort, ploted against results from ChickenGTEx pilot phase. Colored triangles represent ChickenSexGTEx data; grey dots represent ChickenGTEx pilot phase data. The red regression line is modeled on sample size and eGene count per expressed gene from the pilot phase. **(B)** Comparison of eGene count per sample size between ChickenGTEx pilot phase and ChickenSexGTEx. **(C)** Summary of eGene and sGene counts identified in ChickenGTEx pilot phase and ChickenSexGTEx. **(D)** Enrichment analysis of independent eQTL and sQTL in annotated functional elements (left panel) and genomic regions (right panel) across the chicken genome.

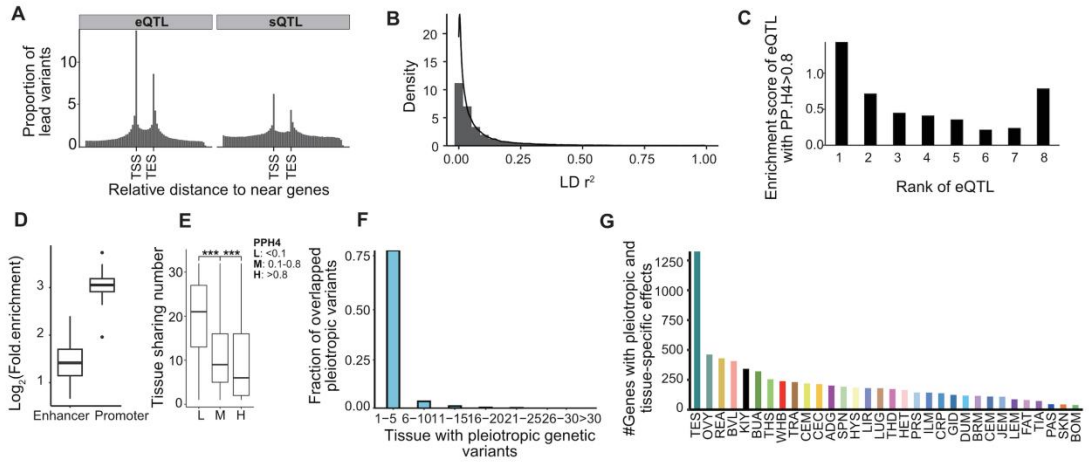

Supplementary Fig. 9. Colocalization of eQTL and sQTL, and characterization of pleiotropic regulatory variants

(A) Proportion of leading eQTL and sQTL plotted against their distance to the TSS and TES of target genes. **(B)** Density distribution of LD between leading eQTL and sQTL. **(C)** Enrichment of pleiotropic regulatory variants across eQTL significance ranks. **(D)** Enrichment of pleiotropic regulatory variants in functionally annotated enhancers and promoters. **(E)** Number of shared tissues for eQTLs stratified by colocalization probability with sQTLs: low (PP.H4 < 0.1), median (0.1 < PP.H4 < 0.8), and high (PP.H4 > 0.8). **(F)** Tissue-sharing pattern of pleiotropic regulatory variants. **(G)** Tissue distribution of tissue-specific pleiotropic variants.

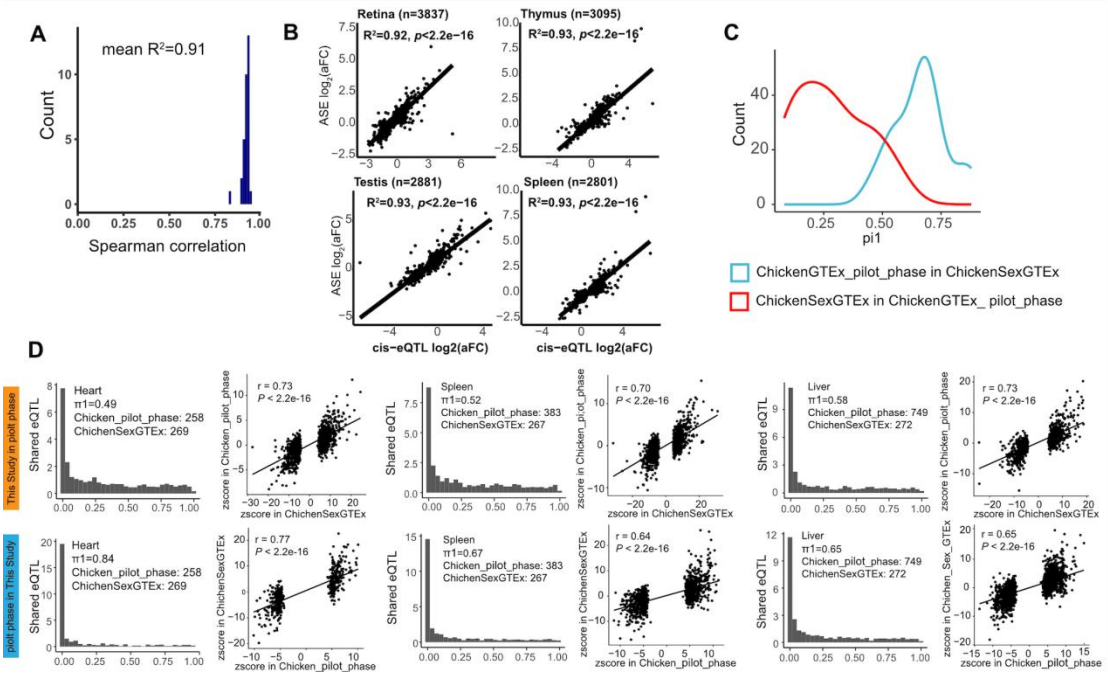

Supplementary Fig. 10. Validation of eQTL across ChickenGTEx pilot phase

(A) Spearman's correlation of eQTL effect sizes estimated via allele-specific expression (ASE) and linear mixed model. **(B)** Concordance of eQTL and ASE effect sizes in representative tissues. **(C)** Cross-validation of eQTL between ChickenSexGTEx cohort and ChickenGTEx pilot phase study. **(D)** eQTL replication rates in the ChickenGTEx pilot phase[1] (top panel) and

ChickenSexGTEx cohort (bottom panel) for heart (left), spleen (middle), and liver (right) tissues. Histograms show the distribution of *P* values for shared eQTL between the two studies; scatter plots show the correlation of adjusted effect sizes for shared eQTL.

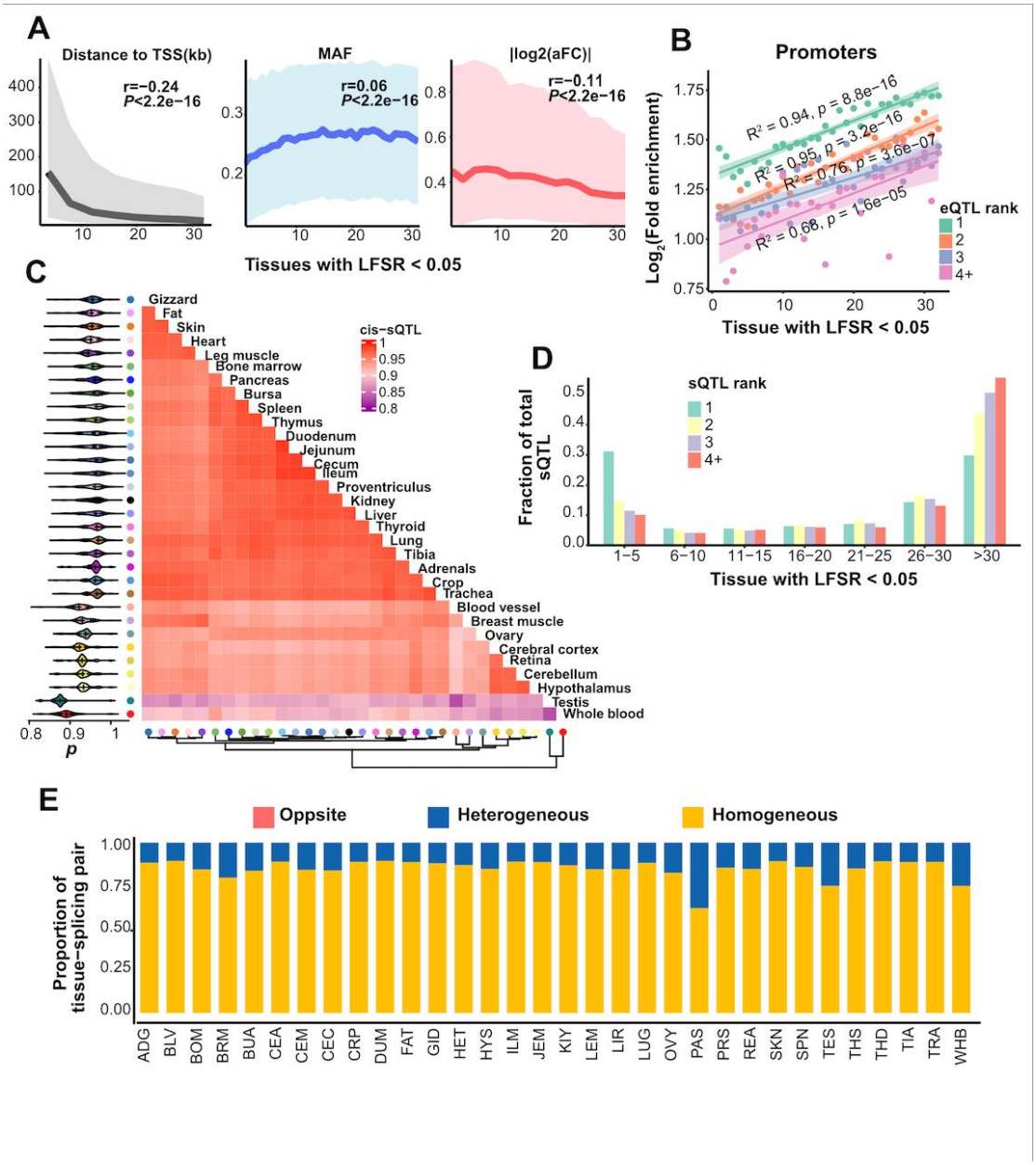

Supplementary Fig. 11. Characterization of tissue-sharing patterns and regulatory features of sQTL

(A) Distance to TSS, MAF, and effect size of eQTLs stratified by the number of shared tissues. **(B)** Enrichment of tissue-shared eQTLs (stratified by significance rank) in functionally annotated promoters. Green dots/lines = rank 1 eQTLs; orange = rank 2; blue = rank 3; purple = rank ≥4. **(C)** Pairwise tissue similarity of sQTL effect sizes, quantified via Spearman's rank correlation. Left panel: distribution of correlation values per tissue; bottom panel: hierarchical clustering of tissues based on regulatory similarity. Tissue types are color-coded as specified in Fig. 2E. **(D)** Fraction of sQTLs shared across varying numbers of tissues (LFSR < 0.05), ranked by

significance from linear mixed models. **(E)** Classification of leading sQTL effects as opposite (red), heterogeneous (blue), or homogeneous (yellow) across tissues.

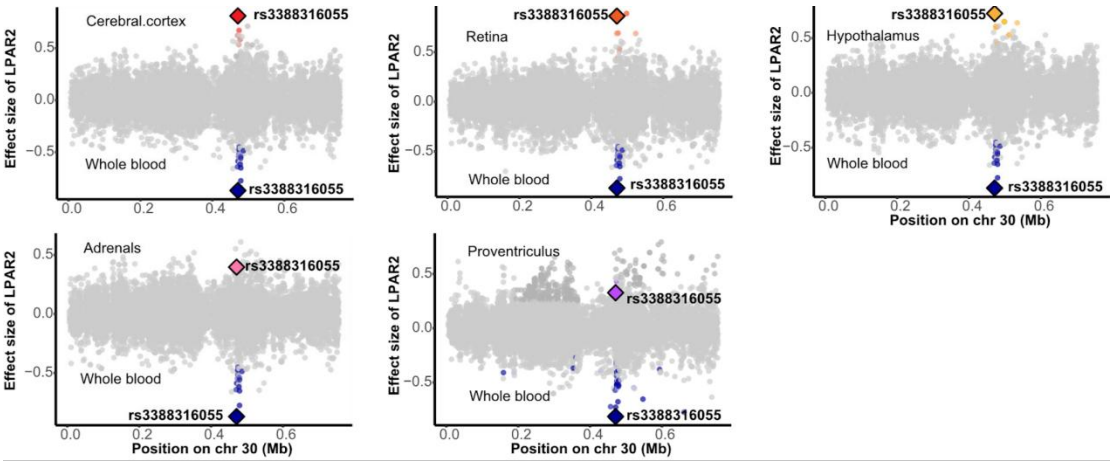

Supplementary Fig. 12. Tissue-specific regulatory effect of variant *rs3388316055* on *LPAR2* expression in whole blood

Effect sizes of regional variants regulating *LPAR2* expression in whole blood (bottom panel) and a contrast panel including cerebral cortex, retina, hypothalamus, adrenal gland, and proventriculus (top panel).

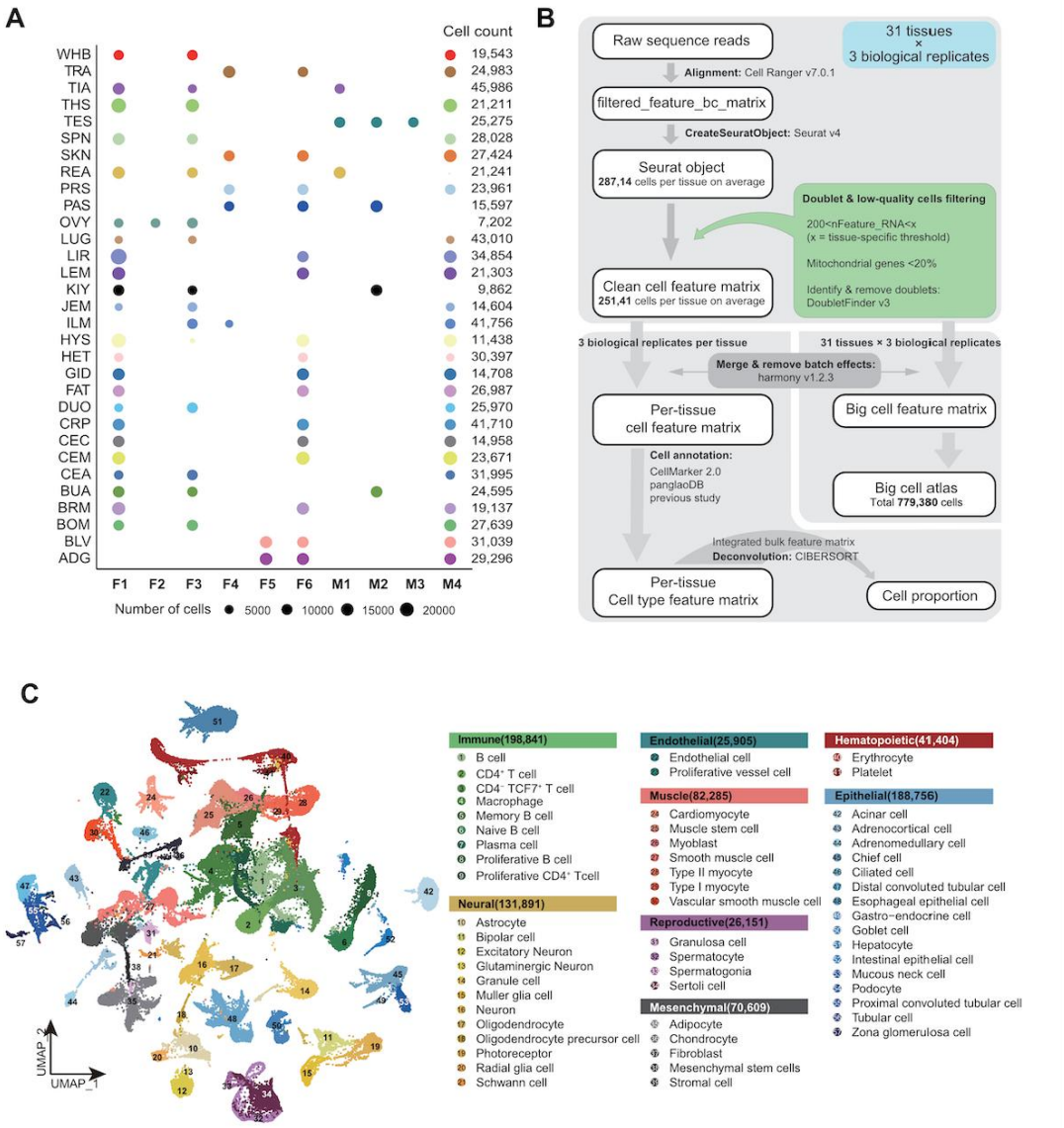

Supplementary Fig. 13. Sample information and preliminary analysis of sc/snRNAseq data **(A)** Tissue sample collection for sc/snRNAseq. Columns represent chicken individuals (1-6 =female; 7-10 = male). Each tissue includes three biological replicates (two female, one male). Total cell counts per tissue are listed in the right column. **(B)** Workflow of sc/snRNAseq data processing: raw sequence alignment, quality control (doublet removal and low-quality cell filtering), batch effect correction, and data integration for cell proportion deconvolution. **(C)** UMAP of 765,842 single cells/nuclei from 31 tissues, annotated into 57 distinct cell types, and categorized into 8 cell groups.

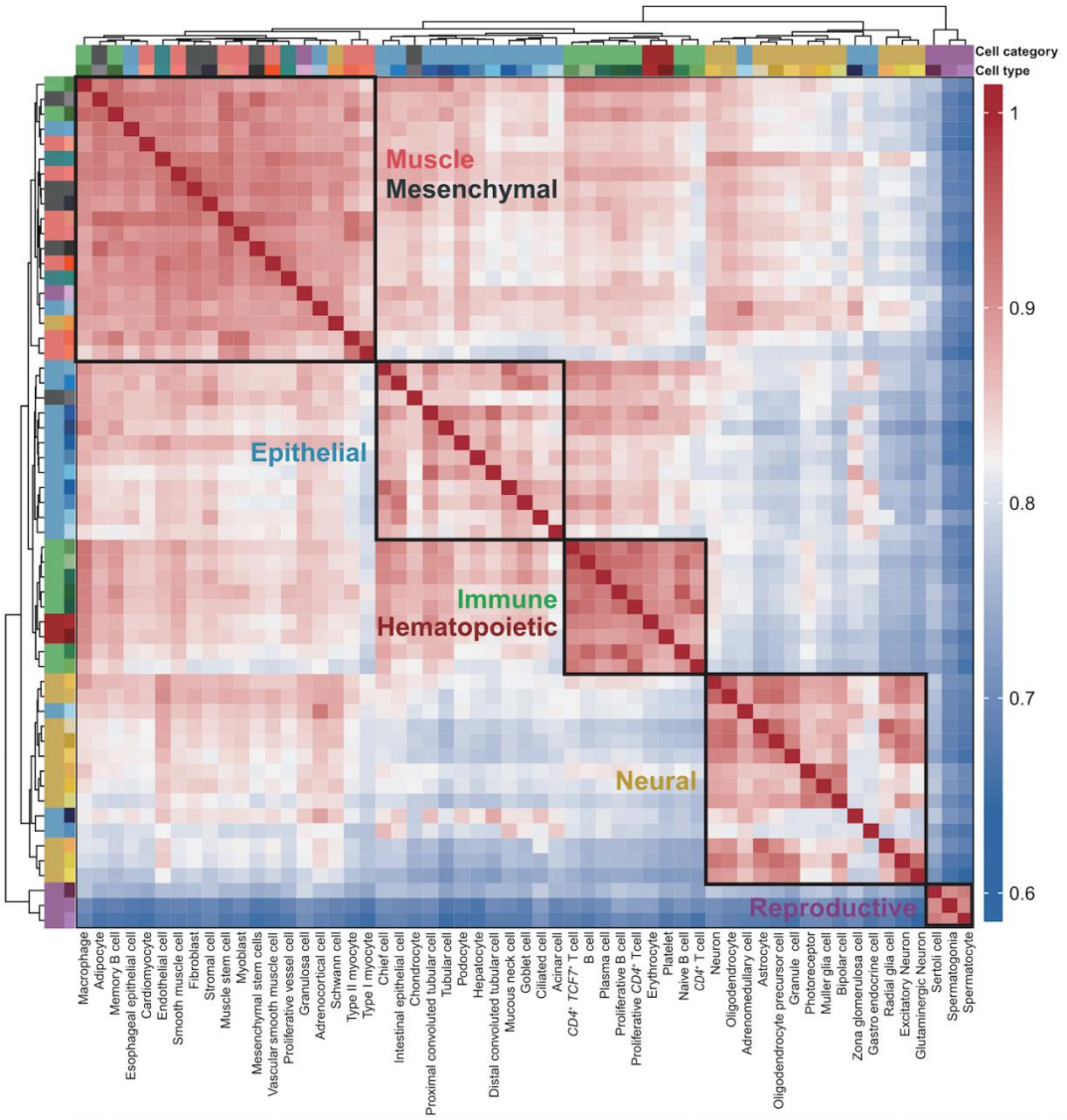

Supplementary Fig. 14. Transcriptomic similarity heatmap of cell types annotated in the single-cell atlas

Heatmap showing transcriptomic similarity between cell types defined in Fig. S13C, across 31 tissues.

Cerebellum

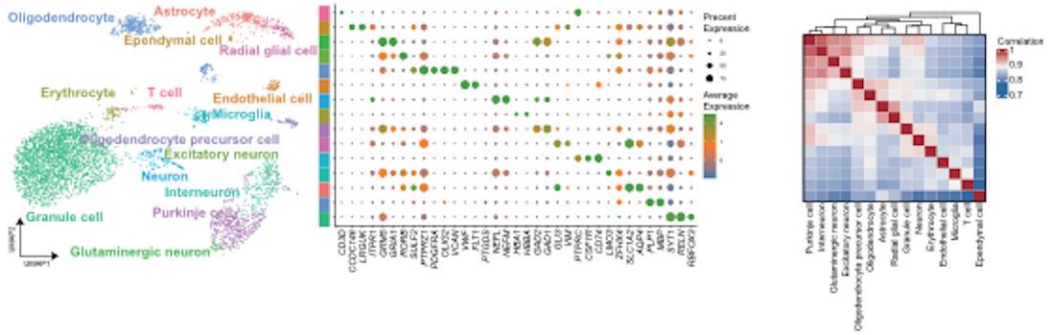

Hypothalamus

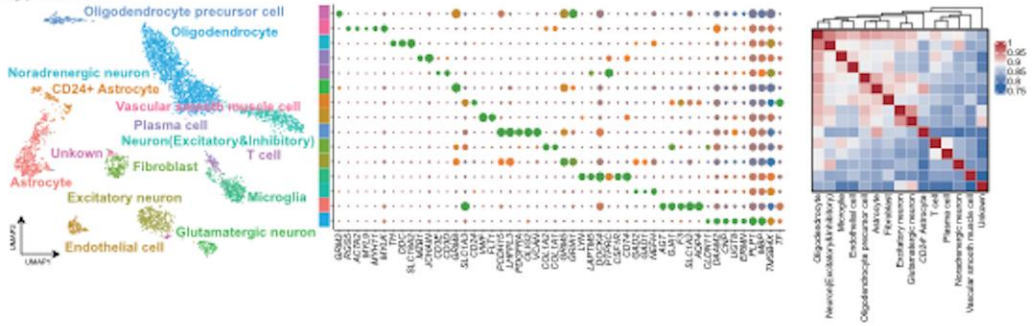

Cerebral cortex

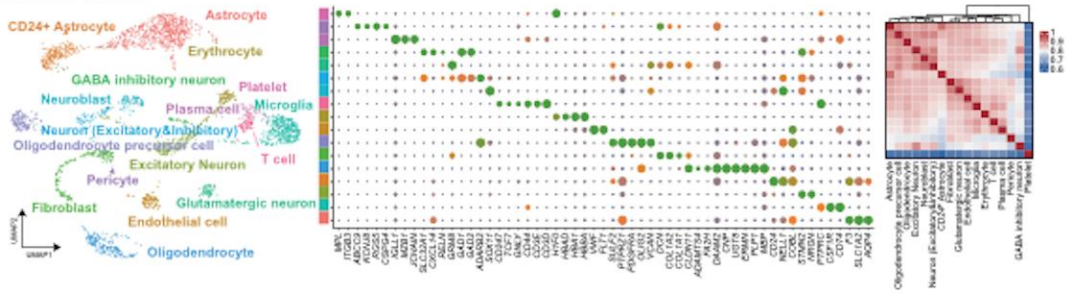

Retina

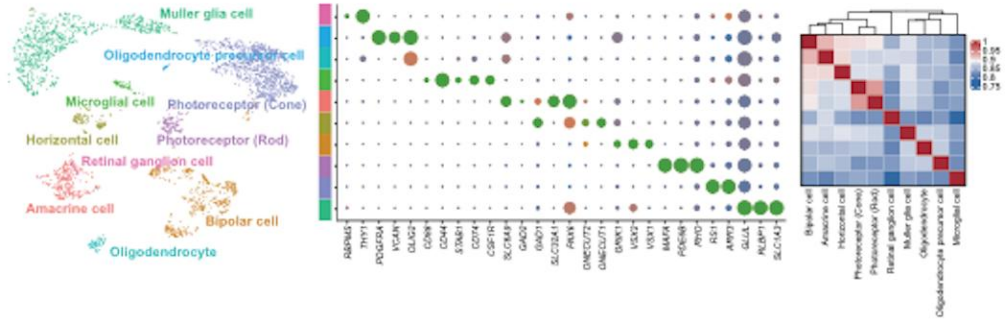

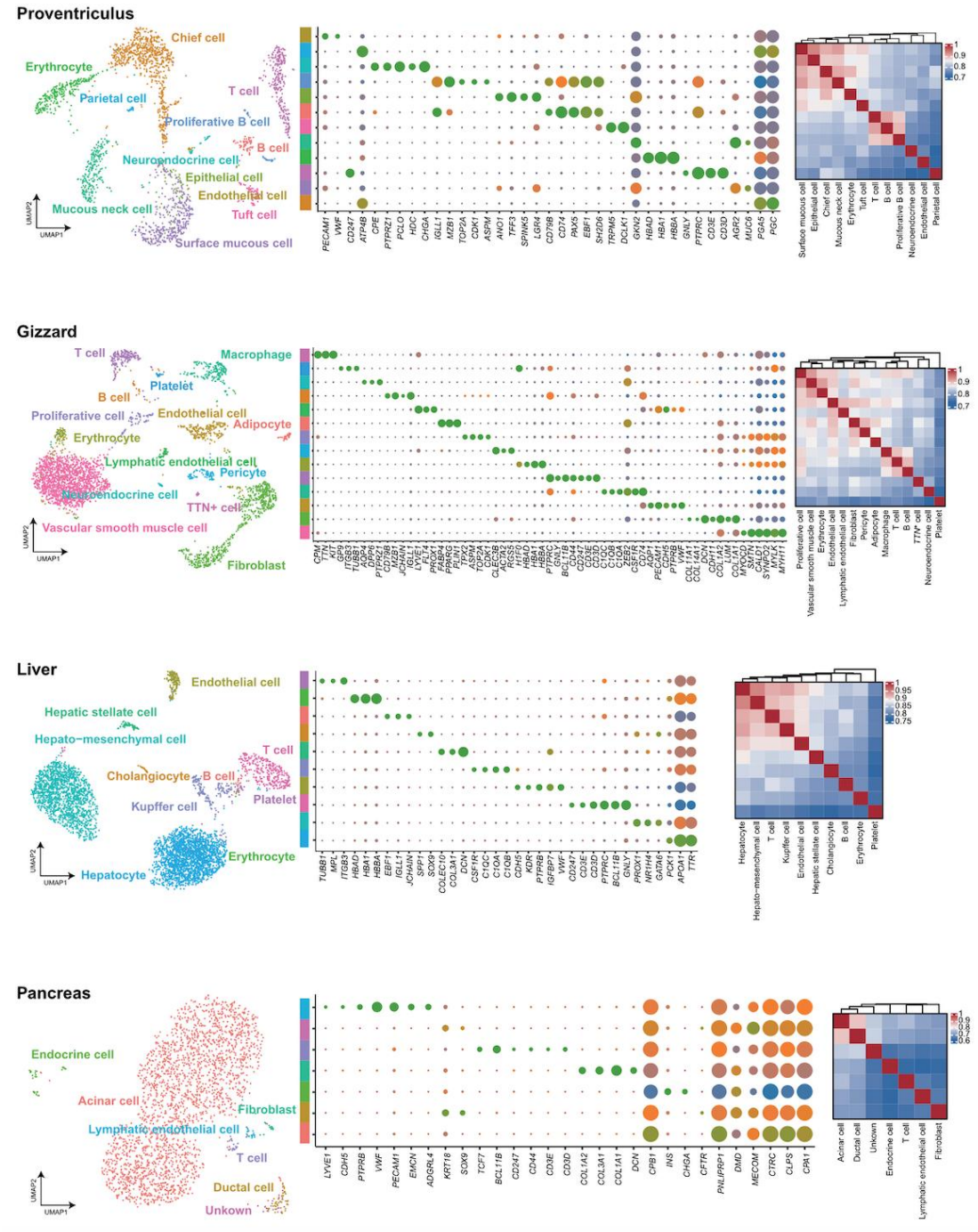
Proventriculus
Chief cell
Erythrocyte
Parietal cell
T cell
Proliferative B cell
B cell
Neuroendocrine cell
Epithelial cell
Endothelial cell
Mucous neck cell
Tuft cell
Surface mucous cell
Gizzard
T cell
Macrophage
Platelet
B cell
Proliferative cell
Endothelial cell
Adipocyte
Erythrocyte
Lymphatic endothelial cell
Pericyte
Neuroendocrine cell
TTN+ cell
Vascular smooth muscle cell
Fibroblast
Liver
Endothelial cell
Hepatic stellate cell
Hepato−mesenchymal cell
T cell
Cholangiocyte
B cell
Platelet
Kupffer cell
Erythrocyte
Hepatocyte
Pancreas
Endocrine cell
Acinar cell
Fibroblast
Lymphatic endothelial cell
T cell
Ductal cell
Unkown
UMAP1
UMAP2

Proventriculus

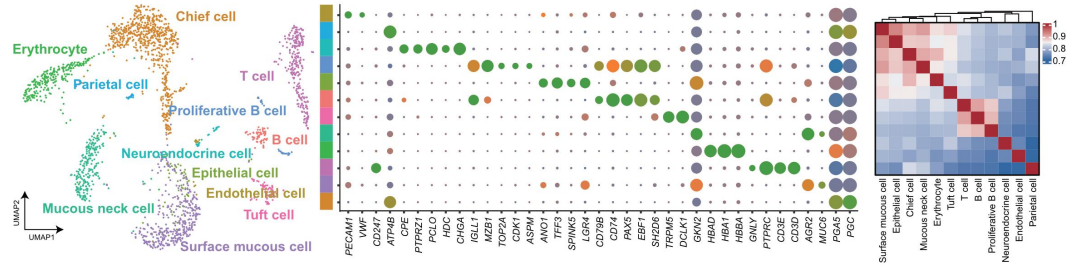

Gizzard

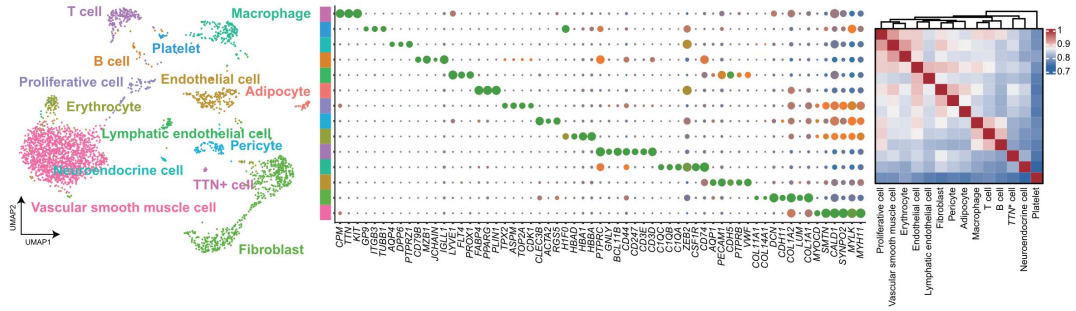

Liver

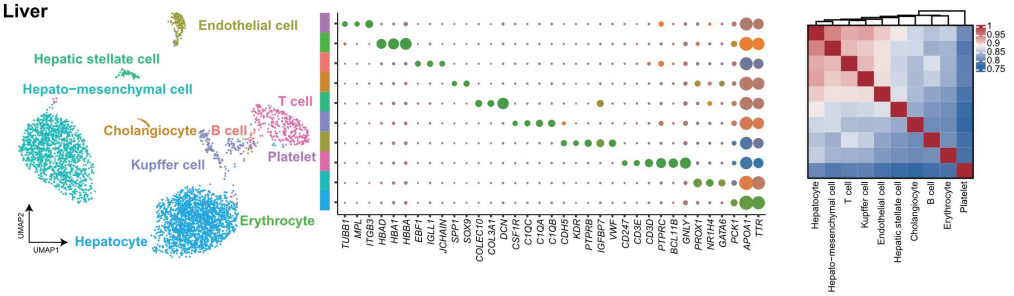

Pancreas

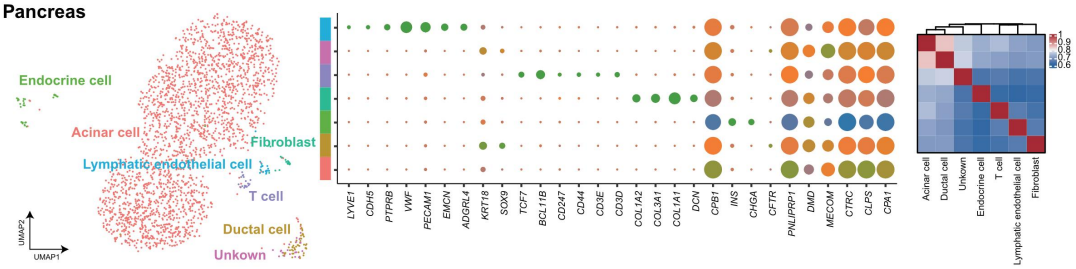

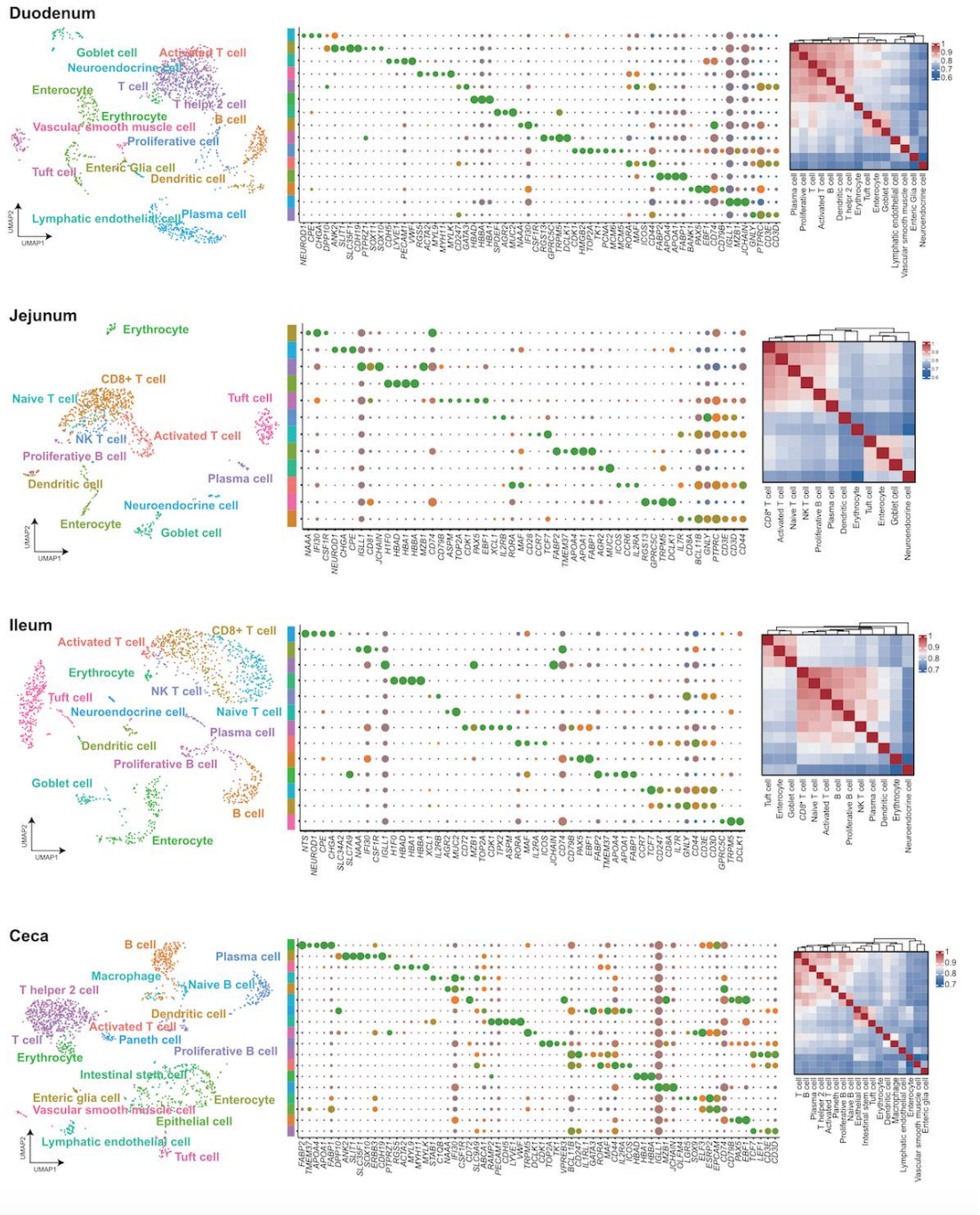
Duodenum
Goblet cell
Activated T cell
Neuroendocrine cell
Enterocyte
T cell
T helper 2 cell
Erythrocyte
B cell
Vascular smooth muscle cell
Proliferative cell
Tuft cell
Enteric Glia cell
Dendritic cell
Lymphatic endothelial cell
Plasma cell
UMAP1
UMAP2
Jejunum
Erythrocyte
CD8+ T cell
Naive T cell
Tuft cell
NK T cell
Activated T cell
Proliferative B cell
Dendritic cell
Plasma cell
Neuroendocrine cell
Enterocyte
Goblet cell
Ileum
Activated T cell
CD8+ T cell
Erythrocyte
NK T cell
Tuft cell
Naive T cell
Neuroendocrine cell
Plasma cell
Dendritic cell
Proliferative B cell
Goblet cell
B cell
Enterocyte
Ceca
B cell
Plasma cell
Macrophage
Naive B cell
T helper 2 cell
Dendritic cell
Activated T cell
T cell
Paneth cell
Erythrocyte
Proliferative B cell
Intestinal stem cell
Enteric glia cell
Enterocyte
Vascular smooth muscle cell
Epithelial cell
Lymphatic endothelial cell
Tuft cell

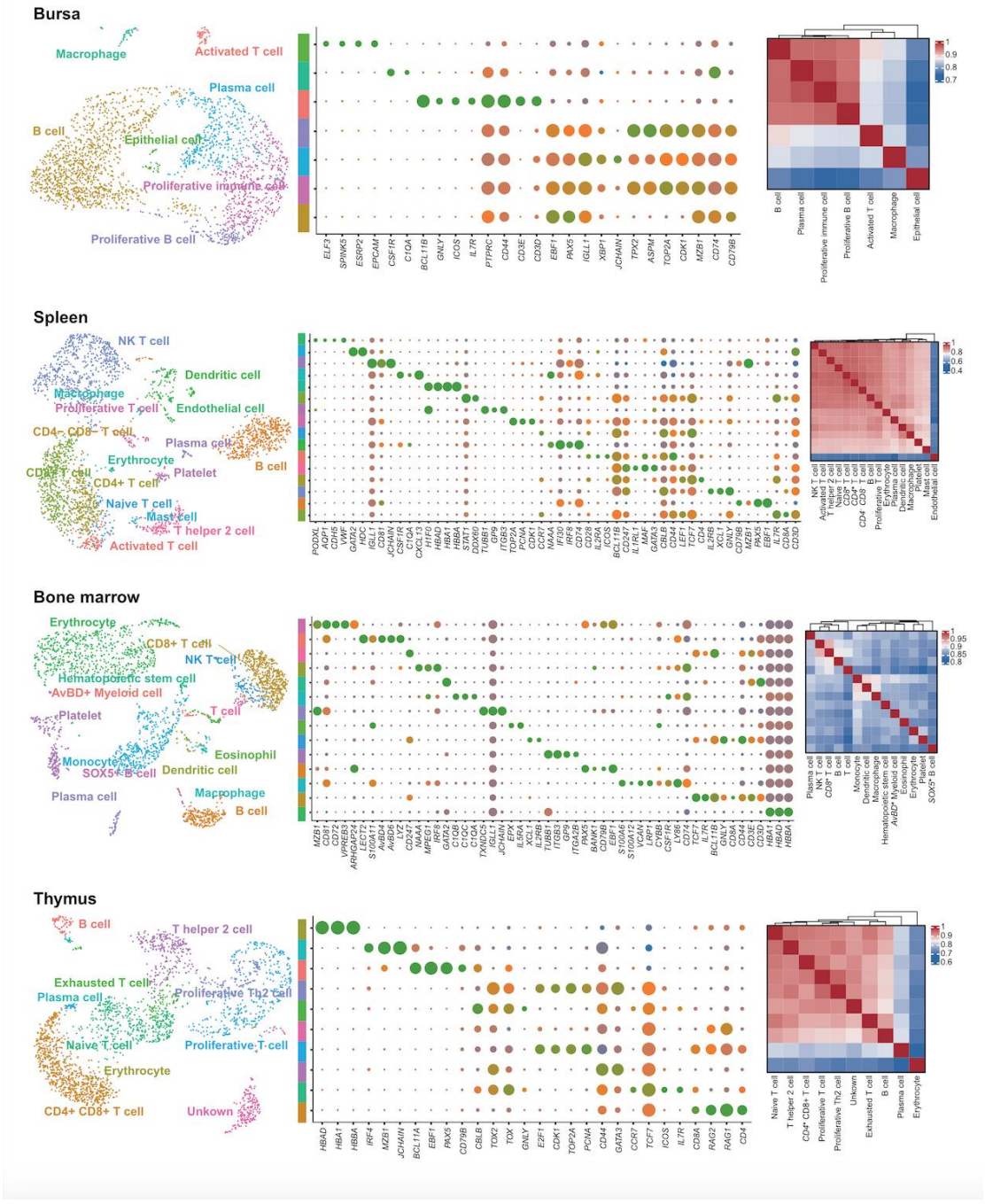
Bursa
Macrophage
Activated T cell
Plasma cell
B cell
Epithelial cell
Proliferative immune cell
Proliferative B cell
Spleen
NK T cell
Dendritic cell
Macrophage
Proliferative T cell
Endothelial cell
CD4- CD8- T cell
Plasma cell
Erythrocyte
CD8+ T cell
Platelet
B cell
CD4+ T cell
Naive T cell
Mast cell
T helper 2 cell
Activated T cell
Bone marrow
Erythrocyte
CD8+ T cell
NK T cell
Hematopoietic stem cell
AvBD+ Myeloid cell
Platelet
T cell
Eosinophil
Monocyte
SOX5+ B cell
Dendritic cell
Plasma cell
Macrophage
B cell
Thymus
B cell
T helper 2 cell
Exhausted T cell
Plasma cell
Proliferative Th2 cell
Naive T cell
Proliferative T cell
Erythrocyte
CD4+ CD8+ T cell
Unkown

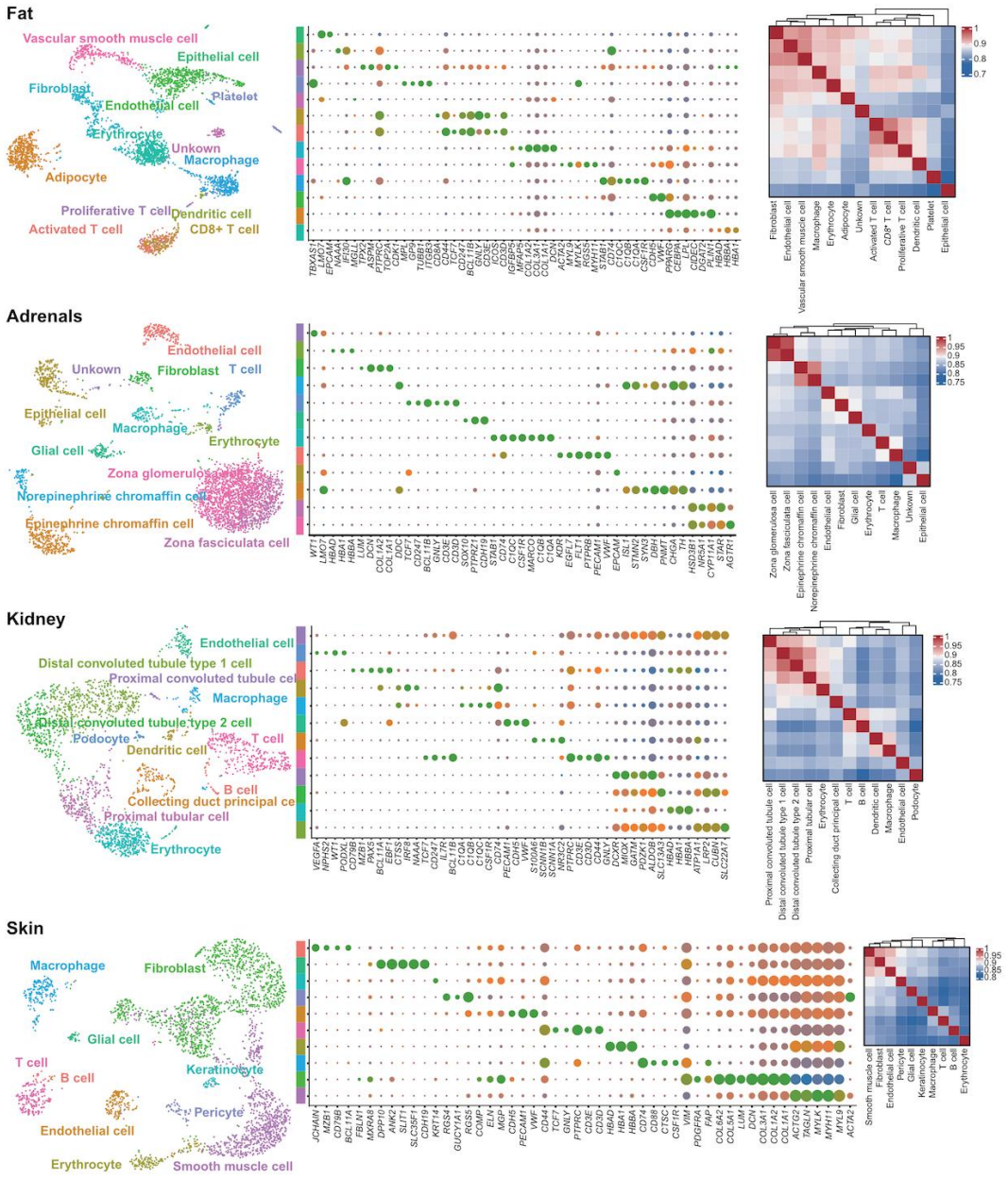
Fat
Vascular smooth muscle cell
Epithelial cell
Fibroblast
Platelet
Endothelial cell
Erythrocyte
Unkown
Macrophage
Adipocyte
Proliferative T cell
Dendritic cell
Activated T cell
CD8+ T cell
Adrenals
Endothelial cell
Unkown
Fibroblast
T cell
Epithelial cell
Macrophage
Erythrocyte
Glial cell
Zona glomerulosa cell
Norepinephrine chromaffin cell
Epinephrine chromaffin cell
Zona fasciculata cell
Kidney
Endothelial cell
Distal convoluted tubule type 1 cell
Proximal convoluted tubule cel
Macrophage
Distal convoluted tubule type 2 cell
Podocyte
Dendritic cell
T cell
B cell
Collecting duct principal ce
Proximal tubular cell
Erythrocyte
Skin
Macrophage
Fibroblast
Glial cell
T cell
B cell
Keratinocyte
Pericyte
Endothelial cell
Erythrocyte
Smooth muscle cell

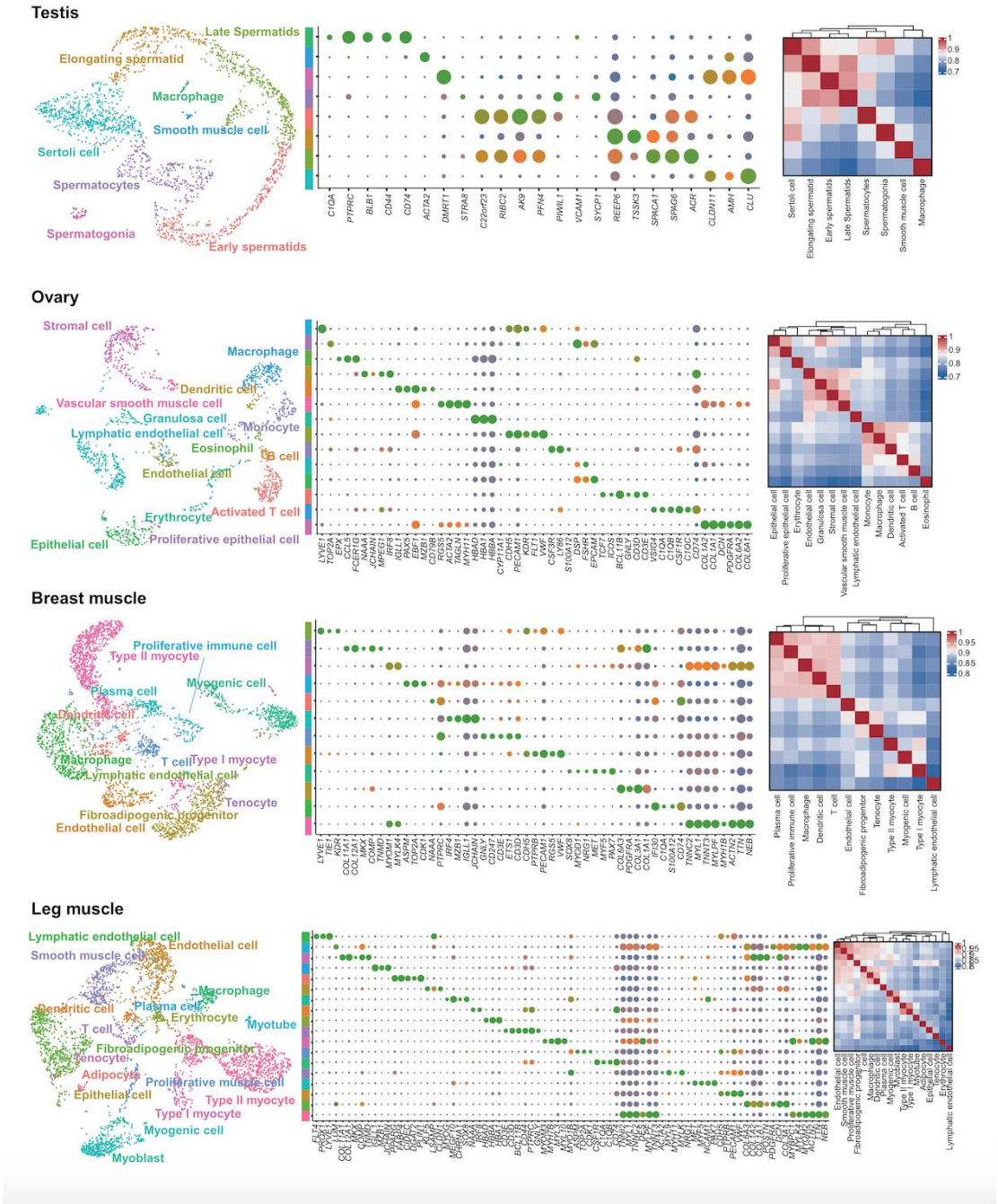
Testis
Late Spermatids
Elongating spermatid
Macrophage
Smooth muscle cell
Sertoli cell
Spermatocytes
Spermatogonia
Early spermatids
C1QA PTPRC BLB1 CD44 CD74 ACTA2 DMRT1 STRA8 C22orf23 RIBC2 AK9 PFN4 PIWIL1 VCAM1 SYCP1 REEP6 TSSK3 SPACA1 SPAG6 ACR CLDN11 AMH CLU
Sertoli cell
Elongating spermatid
Early spermatids
Late Spermatids
Spermatocytes
Spermatogonia
Smooth muscle cell
Macrophage
Ovary
Stromal cell
Macrophage
Dendritic cell
Vascular smooth muscle cell
Granulosa cell
Lymphatic endothelial cell
Monocyte
Eosinophil
B cell
Endothelial cell
Activated T cell
Erythrocyte
Epithelial cell
Proliferative epithelial cell
Epithelial cell
Proliferative epithelial cell
Endothelial cell
Granulosa cell
Stromal cell
Vascular smooth muscle cell
Lymphatic endothelial cell
Monocyte
Macrophage
Dendritic cell
Activated T cell
B cell
Eosinophil
Breast muscle
Proliferative immune cell
Type II myocyte
Myogenic cell
Plasma cell
Dendritic cell
Macrophage
T cell
Type I myocyte
Lymphatic endothelial cell
Tenocyte
Fibroadipogenic progenitor
Endothelial cell
Plasma cell
Proliferative immune cell
Macrophage
Dendritic cell
T cell
Endothelial cell
Fibroadipogenic progenitor
Tenocyte
Type II myocyte
Myogenic cell
Type I myocyte
Lymphatic endothelial cell
Leg muscle
Lymphatic endothelial cell
Endothelial cell
Smooth muscle cell
Macrophage
Dendritic cell
Plasma cell
Erythrocyte
Myotube
T cell
Fibroadipogenic progenitor
Tenocyte
Adipocyte
Proliferative muscle cell
Epithelial cell
Type II myocyte
Type I myocyte
Myogenic cell
Myoblast

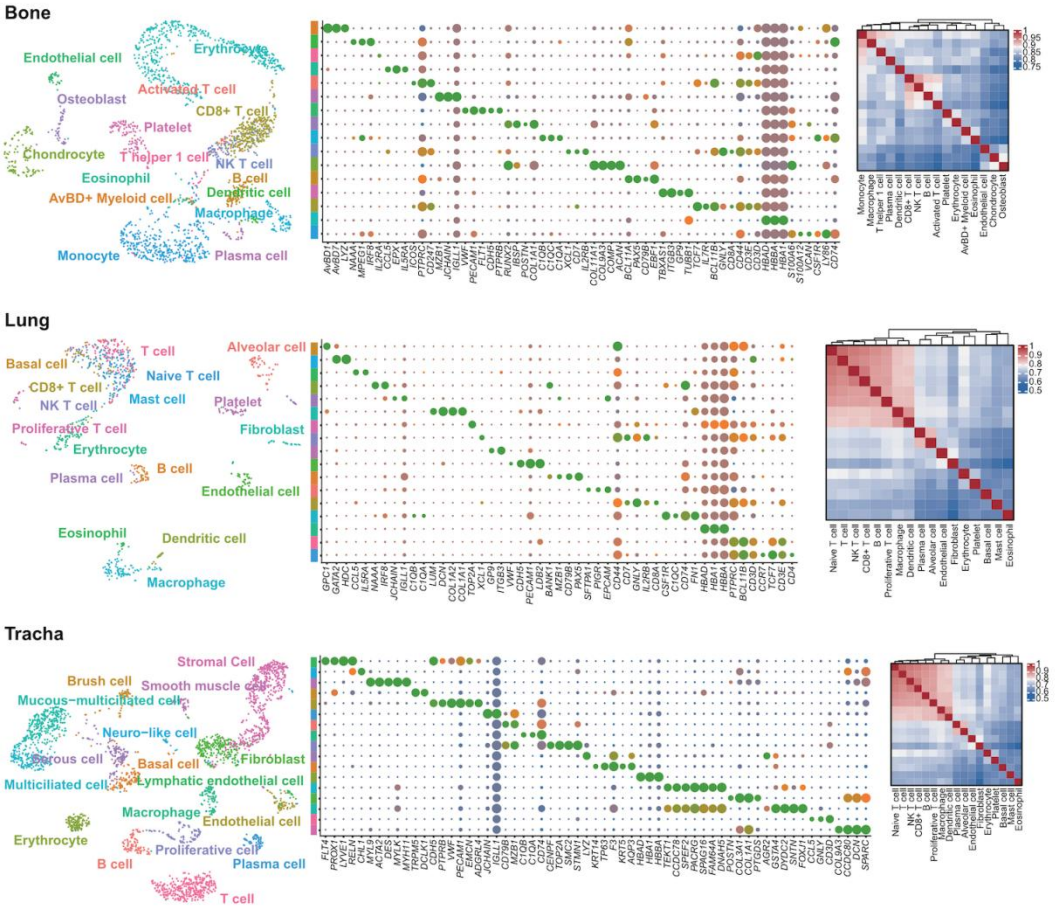

Supplementary Fig. 15 to 22. Single-cell atlas characterization for 31 tissues
For each tissue: UMAP projection of cells (left panel), annotated by marker gene expression (middle panel); transcriptomic similarity of cell types defined in the tissue (right panel).

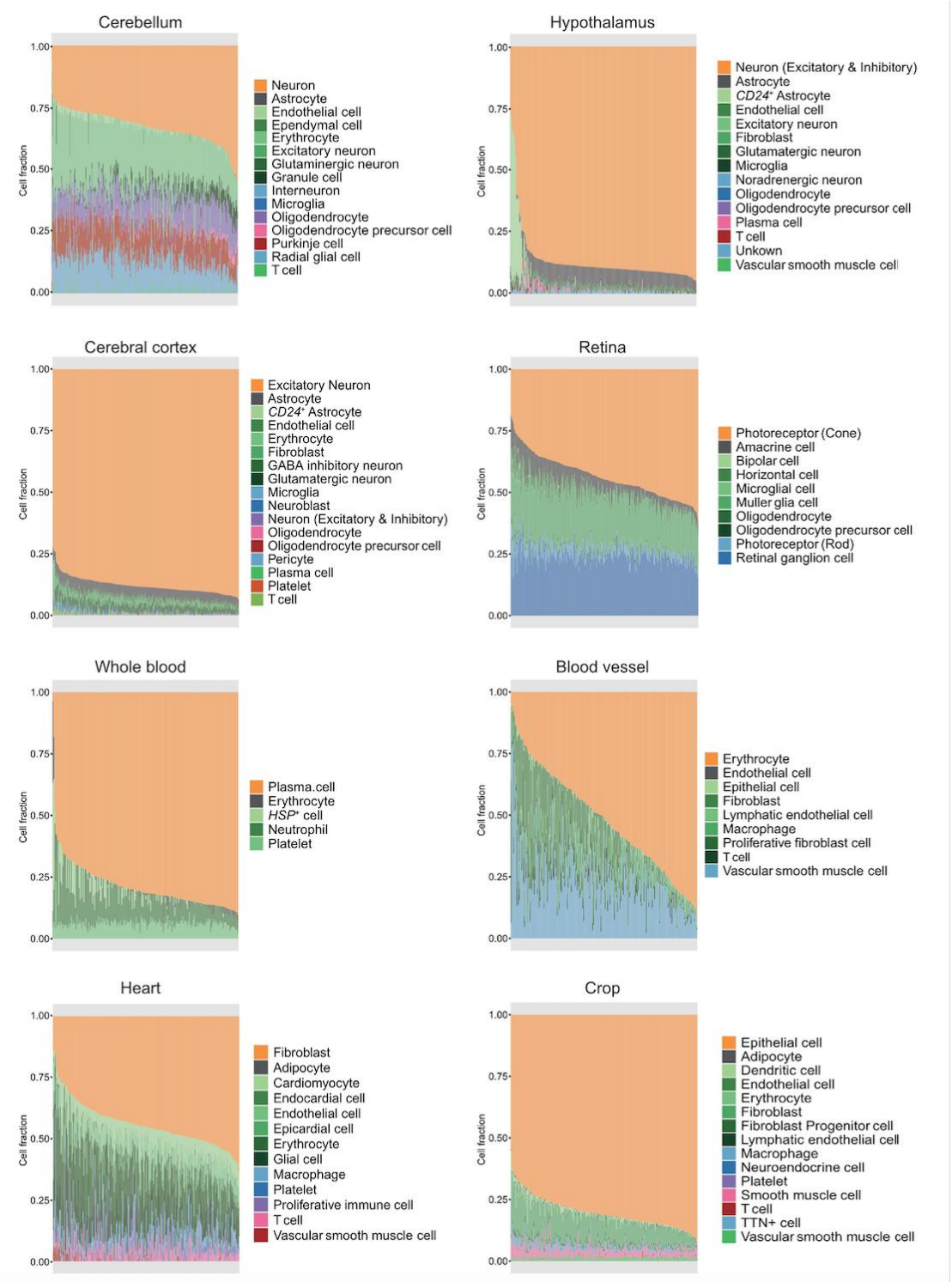
Cerebellum
Cell fraction
1.00
0.75
0.50
0.25
0.00
Neuron
Astrocyte
Endothelial cell
Ependymal cell
Erythrocyte
Excitatory neuron
Glutaminergic neuron
Granule cell
Interneuron
Microglia
Oligodendrocyte
Oligodendrocyte precursor cell
Purkinje cell
Radial glial cell
T cell
Hypothalamus
Cell fraction
1.00
0.75
0.50
0.25
0.00
Neuron (Excitatory & Inhibitory)
Astrocyte
CD24+ Astrocyte
Endothelial cell
Excitatory neuron
Fibroblast
Glutamatergic neuron
Microglia
Noradrenergic neuron
Oligodendrocyte
Oligodendrocyte precursor cell
Plasma cell
T cell
Unkown
Vascular smooth muscle cell
Cerebral cortex
Cell fraction
1.00
0.75
0.50
0.25
0.00
Excitatory Neuron
Astrocyte
CD24+ Astrocyte
Endothelial cell
Erythrocyte
Fibroblast
GABA inhibitory neuron
Glutamatergic neuron
Microglia
Neuroblast
Neuron (Excitatory & Inhibitory)
Oligodendrocyte
Oligodendrocyte precursor cell
Pericyte
Plasma cell
Platelet
T cell
Retina
Cell fraction
1.00
0.75
0.50
0.25
0.00
Photoreceptor (Cone)
Amacrine cell
Bipolar cell
Horizontal cell
Microglial cell
Muller glia cell
Oligodendrocyte
Oligodendrocyte precursor cell
Photoreceptor (Rod)
Retinal ganglion cell
Whole blood
Cell fraction
1.00
0.75
0.50
0.25
0.00
Plasma.cell
Erythrocyte
HSP+ cell
Neutrophil
Platelet
Blood vessel
Cell fraction
1.00
0.75
0.50
0.25
0.00
Erythrocyte
Endothelial cell
Epithelial cell
Fibroblast
Lymphatic endothelial cell
Macrophage
Proliferative fibroblast cell
T cell
Vascular smooth muscle cell
Heart
Cell fraction
1.00
0.75
0.50
0.25
0.00
Fibroblast
Adipocyte
Cardiomyocyte
Endocardial cell
Endothelial cell
Epicardial cell
Erythrocyte
Glial cell
Macrophage
Platelet
Proliferative immune cell
T cell
Vascular smooth muscle cell
Crop
Cell fraction
1.00
0.75
0.50
0.25
0.00
Epithelial cell
Adipocyte
Dendritic cell
Endothelial cell
Erythrocyte
Fibroblast
Fibroblast Progenitor cell
Lymphatic endothelial cell
Macrophage
Neuroendocrine cell
Platelet
Smooth muscle cell
T cell
TTN+ cell
Vascular smooth muscle cell

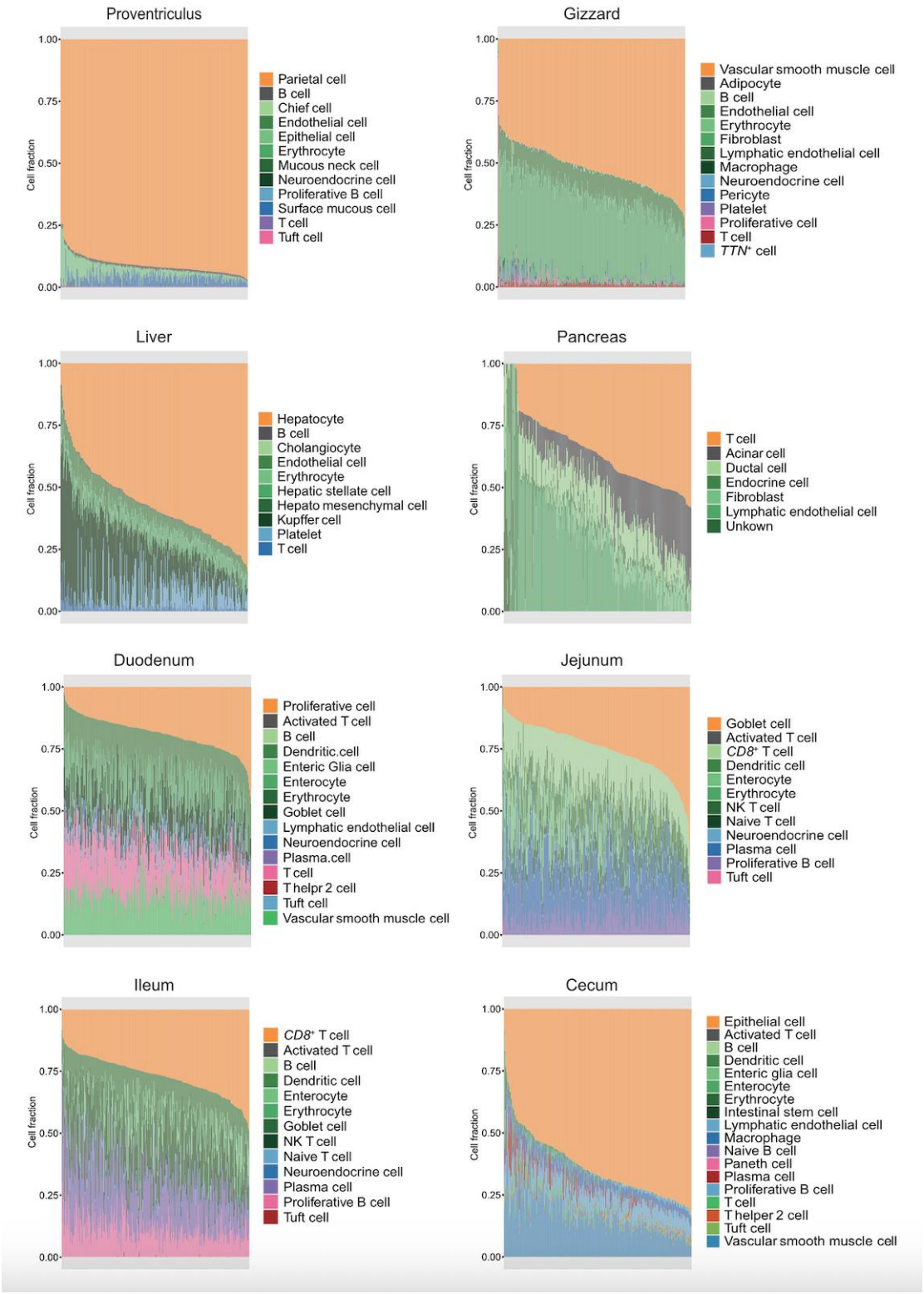
Proventriculus
Cell fraction
1.00
0.75
0.50
0.25
0.00
Parietal cell
B cell
Chief cell
Endothelial cell
Epithelial cell
Erythrocyte
Mucous neck cell
Neuroendocrine cell
Proliferative B cell
Surface mucous cell
T cell
Tuft cell
Gizzard
Vascular smooth muscle cell
Adipocyte
B cell
Endothelial cell
Erythrocyte
Fibroblast
Lymphatic endothelial cell
Macrophage
Neuroendocrine cell
Pericyte
Platelet
Proliferative cell
T cell
TTN+ cell
Liver
Hepatocyte
B cell
Cholangiocyte
Endothelial cell
Erythrocyte
Hepatic stellate cell
Hepato mesenchymal cell
Kupffer cell
Platelet
T cell
Pancreas
T cell
Acinar cell
Ductal cell
Endocrine cell
Fibroblast
Lymphatic endothelial cell
Unkown
Duodenum
Proliferative cell
Activated T cell
B cell
Dendritic.cell
Enteric Glia cell
Enterocyte
Erythrocyte
Goblet cell
Lymphatic endothelial cell
Neuroendocrine cell
Plasma.cell
T cell
T helpr 2 cell
Tuft cell
Vascular smooth muscle cell
Jejunum
Goblet cell
Activated T cell
CD8+ T cell
Dendritic cell
Enterocyte
Erythrocyte
NK T cell
Naive T cell
Neuroendocrine cell
Plasma cell
Proliferative B cell
Tuft cell
Ileum
CD8+ T cell
Activated T cell
B cell
Dendritic cell
Enterocyte
Erythrocyte
Goblet cell
NK T cell
Naive T cell
Neuroendocrine cell
Plasma cell
Proliferative B cell
Tuft cell
Cecum
Epithelial cell
Activated T cell
B cell
Dendritic cell
Enteric glia cell
Enterocyte
Erythrocyte
Intestinal stem cell
Lymphatic endothelial cell
Macrophage
Naive B cell
Paneth cell
Plasma cell
Proliferative B cell
T cell
T helper 2 cell
Tuft cell
Vascular smooth muscle cell

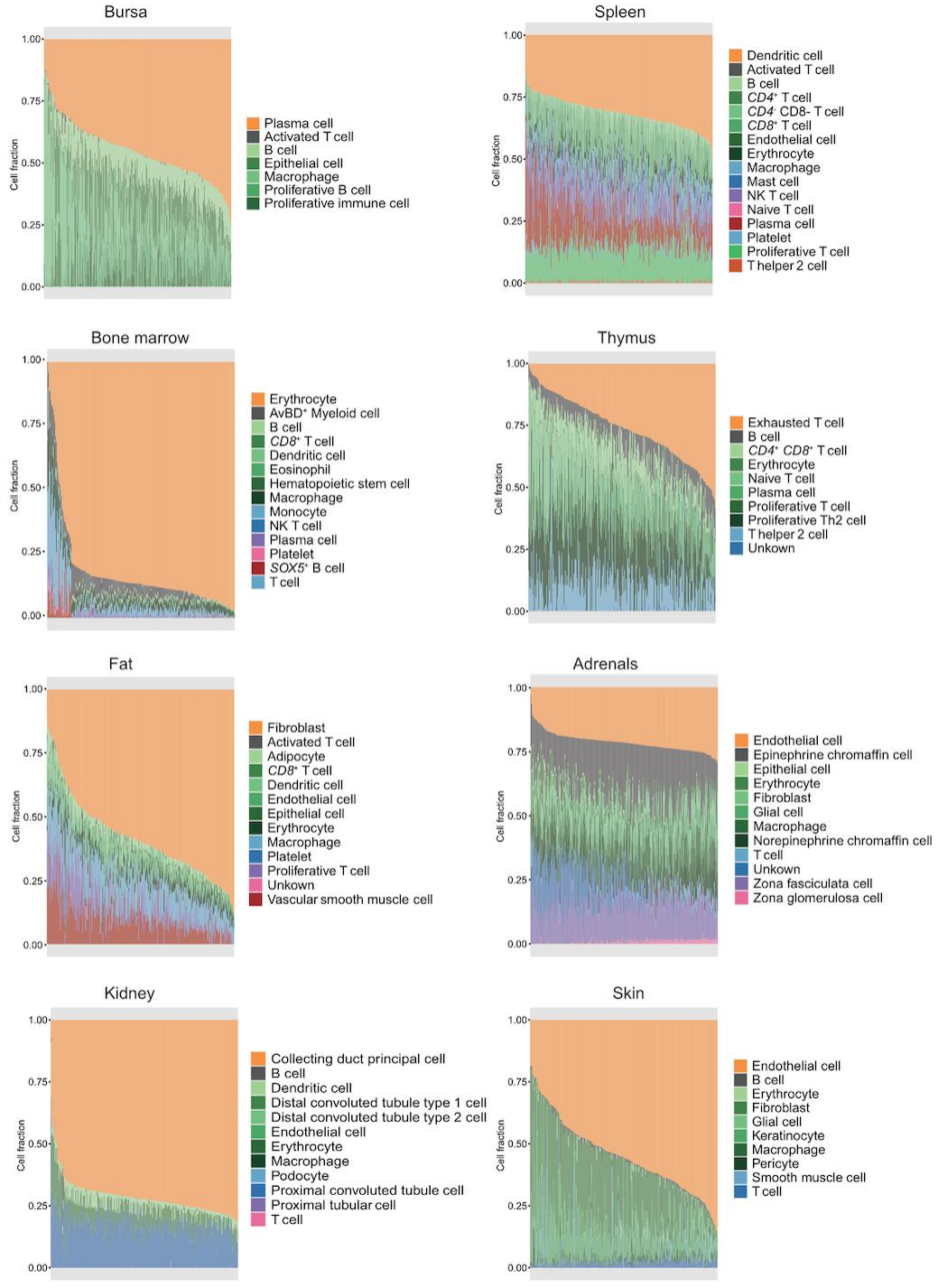
Bursa
Cell fraction
1.00
0.75
0.50
0.25
0.00
Plasma cell
Activated T cell
B cell
Epithelial cell
Macrophage
Proliferative B cell
Proliferative immune cell
Spleen
Dendritic cell
Activated T cell
B cell
CD4+ T cell
CD4- CD8- T cell
CD8+ T cell
Endothelial cell
Erythrocyte
Macrophage
Mast cell
NK T cell
Naive T cell
Plasma cell
Platelet
Proliferative T cell
T helper 2 cell
Bone marrow
Erythrocyte
AvBD+ Myeloid cell
B cell
CD8+ T cell
Dendritic cell
Eosinophil
Hematopoietic stem cell
Macrophage
Monocyte
NK T cell
Plasma cell
Platelet
SOX5+ B cell
T cell
Thymus
Exhausted T cell
B cell
CD4+ CD8+ T cell
Erythrocyte
Naive T cell
Plasma cell
Proliferative T cell
Proliferative Th2 cell
T helper 2 cell
Unkown
Fat
Fibroblast
Activated T cell
Adipocyte
CD8+ T cell
Dendritic cell
Endothelial cell
Epithelial cell
Erythrocyte
Macrophage
Platelet
Proliferative T cell
Unkown
Vascular smooth muscle cell
Adrenals
Endothelial cell
Epinephrine chromaffin cell
Epithelial cell
Erythrocyte
Fibroblast
Glial cell
Macrophage
Norepinephrine chromaffin cell
T cell
Unkown
Zona fasciculata cell
Zona glomerulosa cell
Kidney
Collecting duct principal cell
B cell
Dendritic cell
Distal convoluted tubule type 1 cell
Distal convoluted tubule type 2 cell
Endothelial cell
Erythrocyte
Macrophage
Podocyte
Proximal convoluted tubule cell
Proximal tubular cell
T cell
Skin
Endothelial cell
B cell
Erythrocyte
Fibroblast
Glial cell
Keratinocyte
Macrophage
Pericyte
Smooth muscle cell
T cell

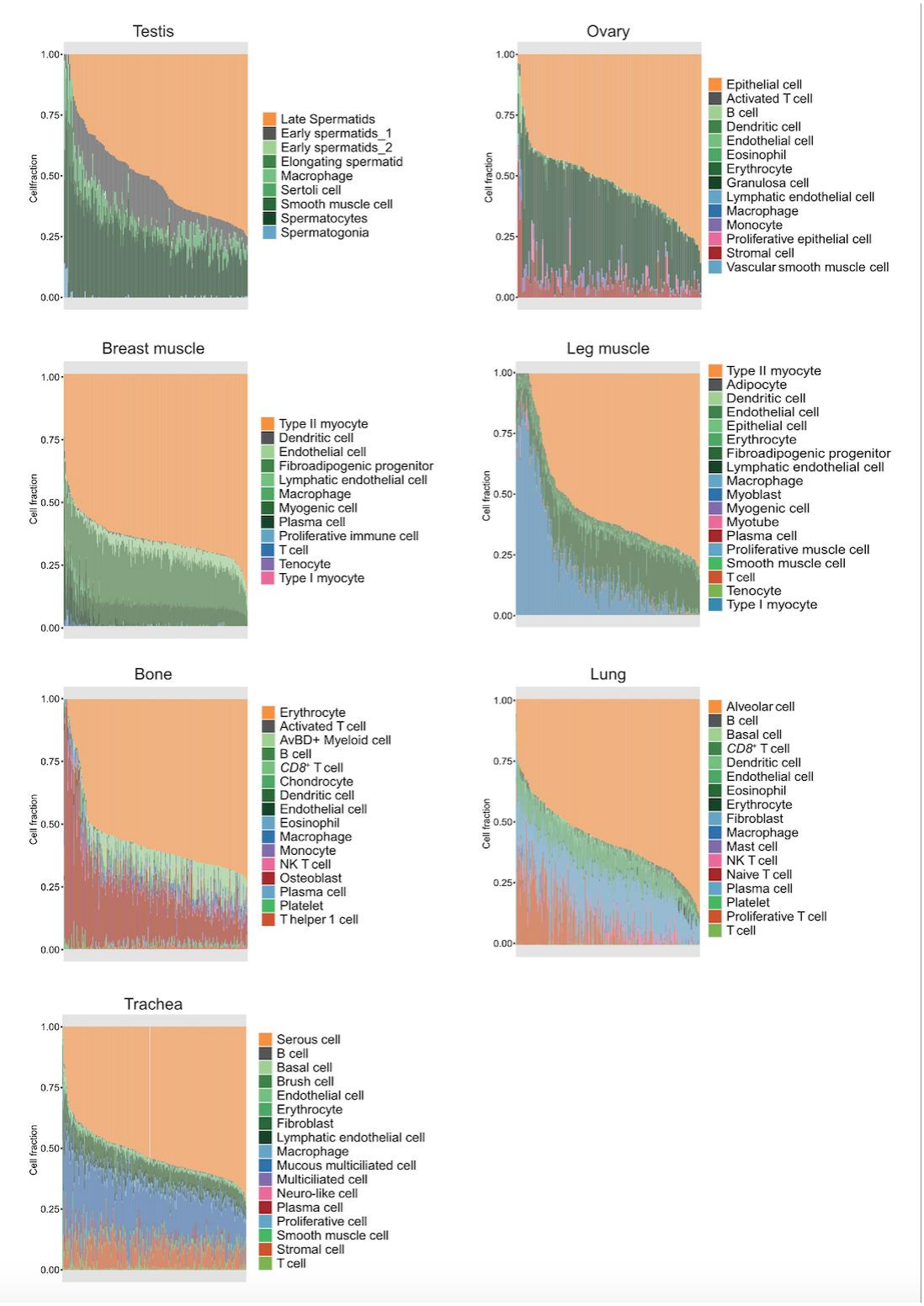

Supplementary Fig. 23 to 26. Cell type proportion deconvolution across the 280-individual ChickenSexGTEx cohort

For each tissue: columns represent individual chickens; cell type proportions are color-coded according to the cell type annotations for the tissue.

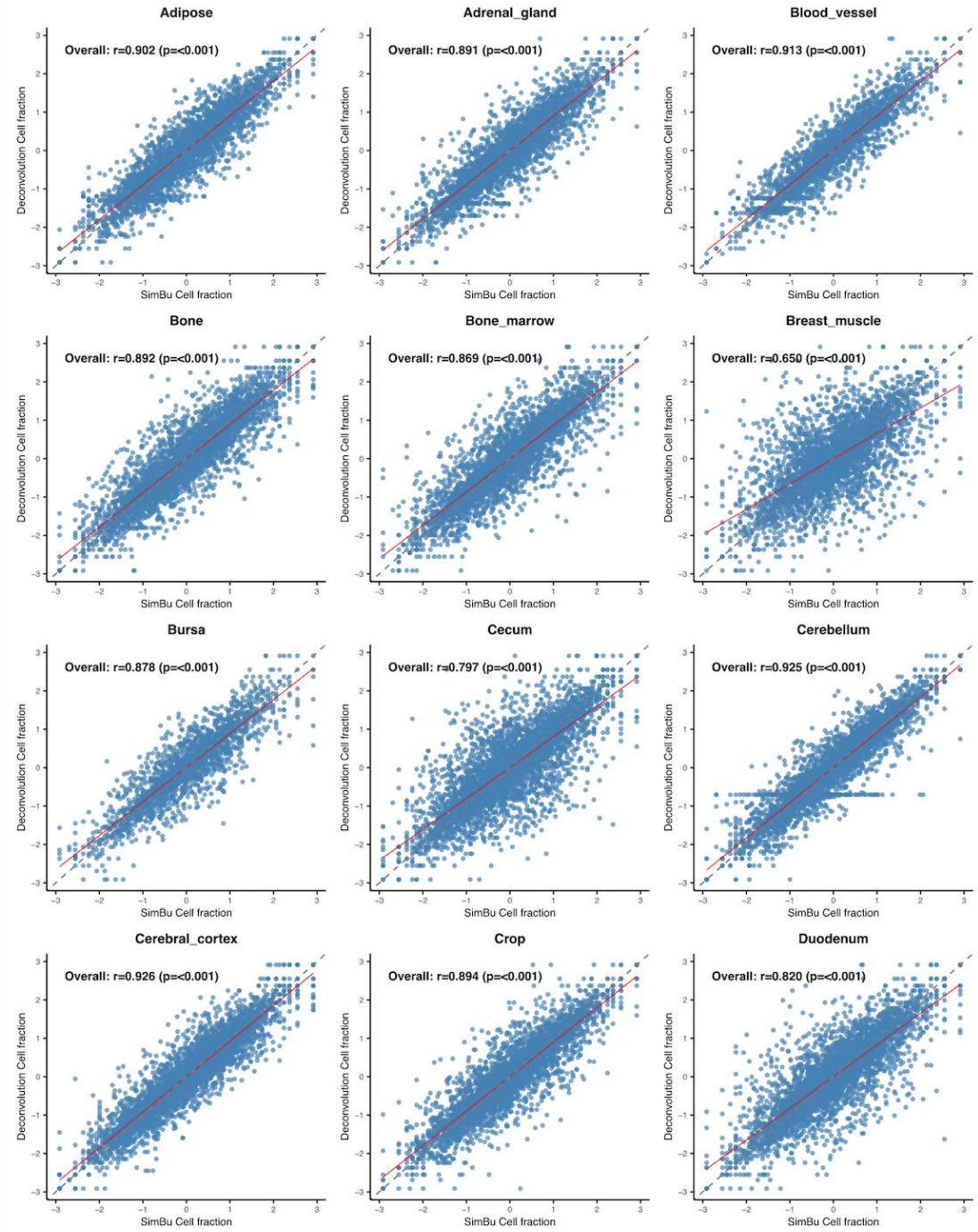
Adipose
Overall: r=0.902 (p=<0.001)
Adrenal_gland
Overall: r=0.891 (p=<0.001)
Blood_vessel
Overall: r=0.913 (p=<0.001)
Bone
Overall: r=0.892 (p=<0.001)
Bone_marrow
Overall: r=0.869 (p=<0.001)
Breast_muscle
Overall: r=0.650 (p=<0.001)
Bursa
Overall: r=0.878 (p=<0.001)
Cecum
Overall: r=0.797 (p=<0.001)
Cerebellum
Overall: r=0.925 (p=<0.001)
Cerebral_cortex
Overall: r=0.926 (p=<0.001)
Crop
Overall: r=0.894 (p=<0.001)
Duodenum
Overall: r=0.820 (p=<0.001)
Deconvolution Cell fraction
SimBu Cell fraction

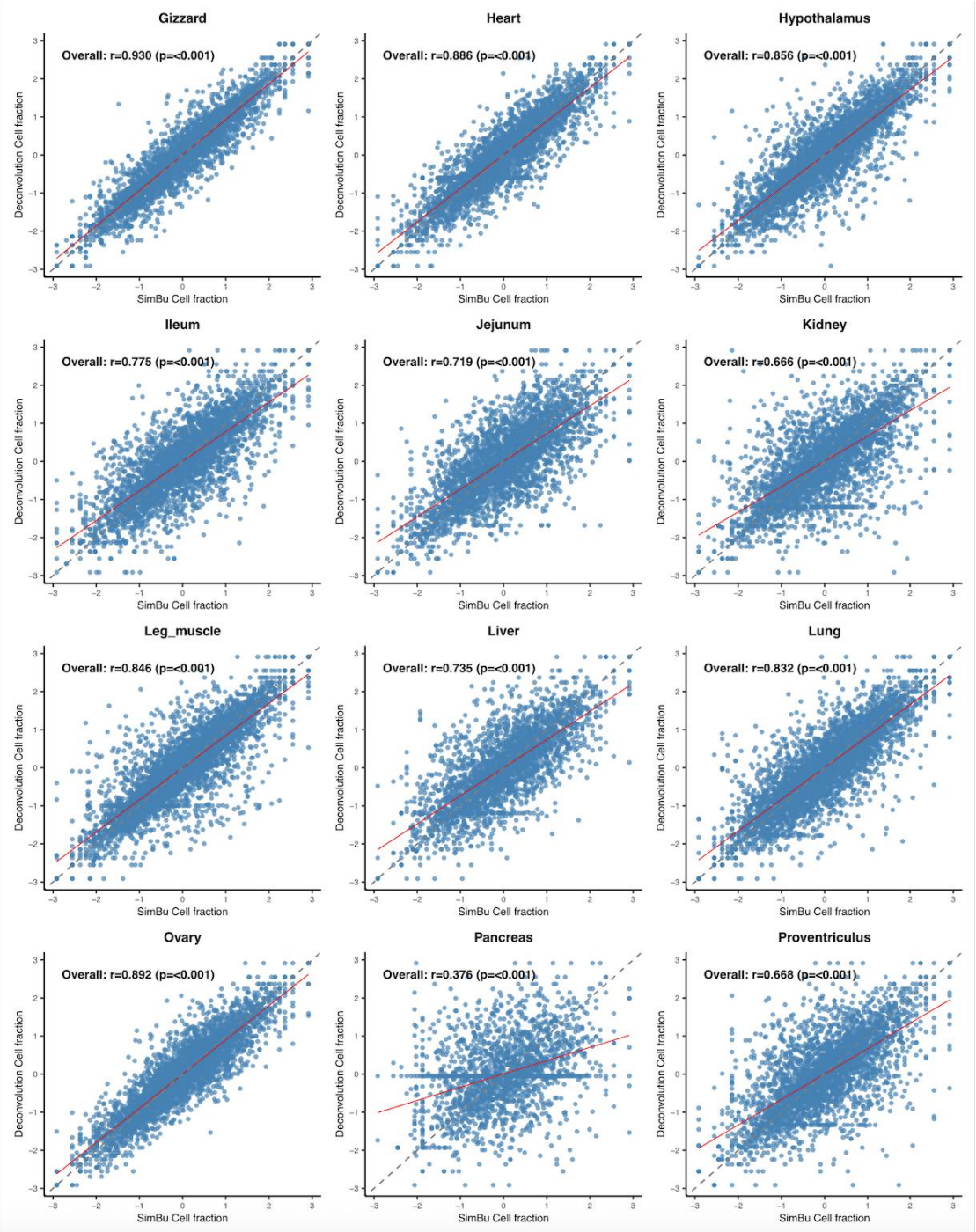
Gizzard
Overall: r=0.930 (p=<0.001)
Heart
Overall: r=0.886 (p=<0.001)
Hypothalamus
Overall: r=0.856 (p=<0.001)
Ileum
Overall: r=0.775 (p=<0.001)
Jejunum
Overall: r=0.719 (p=<0.001)
Kidney
Overall: r=0.666 (p=<0.001)
Leg_muscle
Overall: r=0.846 (p=<0.001)
Liver
Overall: r=0.735 (p=<0.001)
Lung
Overall: r=0.832 (p=<0.001)
Ovary
Overall: r=0.892 (p=<0.001)
Pancreas
Overall: r=0.376 (p=<0.001)
Proventriculus
Overall: r=0.668 (p=<0.001)
Deconvolution Cell fraction
SimBu Cell fraction

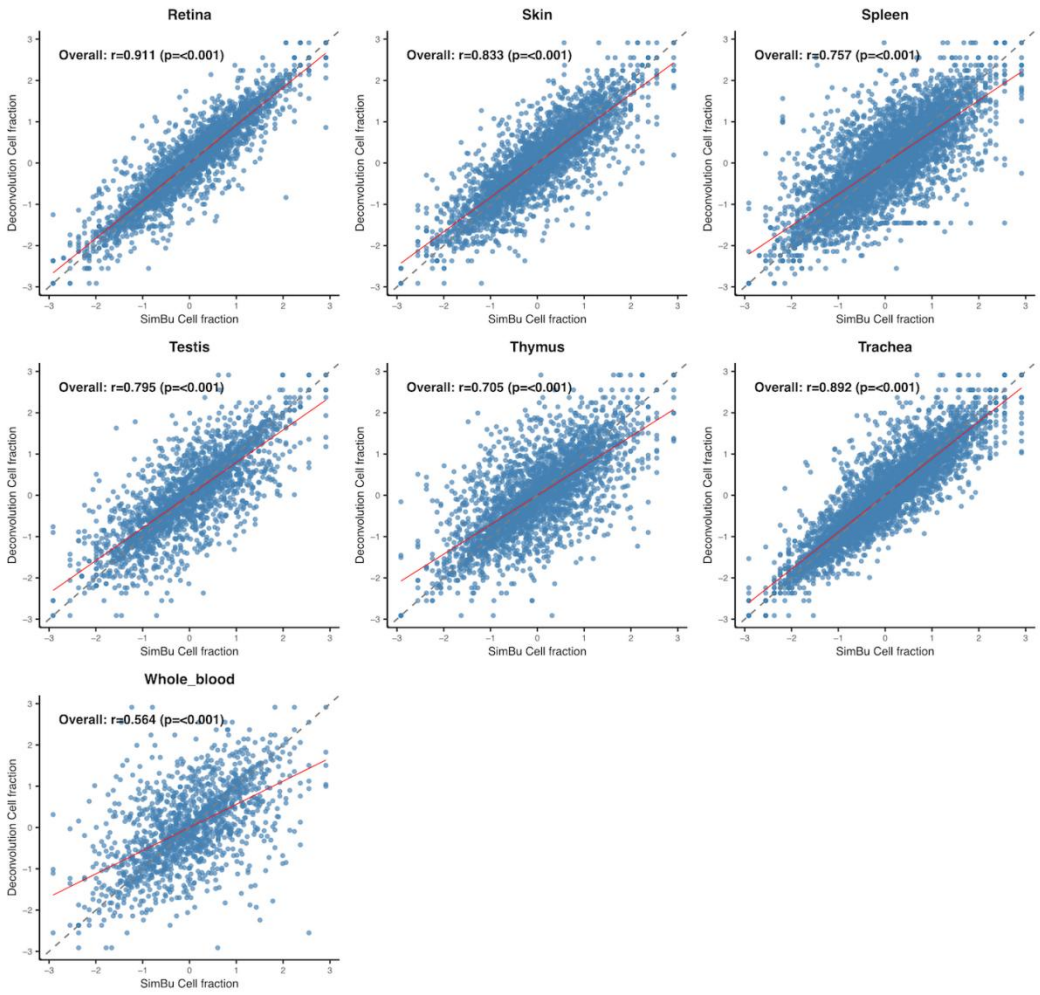

Supplementary Fig. 27 to 29. Validation of cell fraction deconvolution accuracy
Pearson's correlation between deconvoluted cell fractions and true cell fractions from simulated scRNA-seq data. Simulations were performed using SimBu[2] (1.2.0) software.

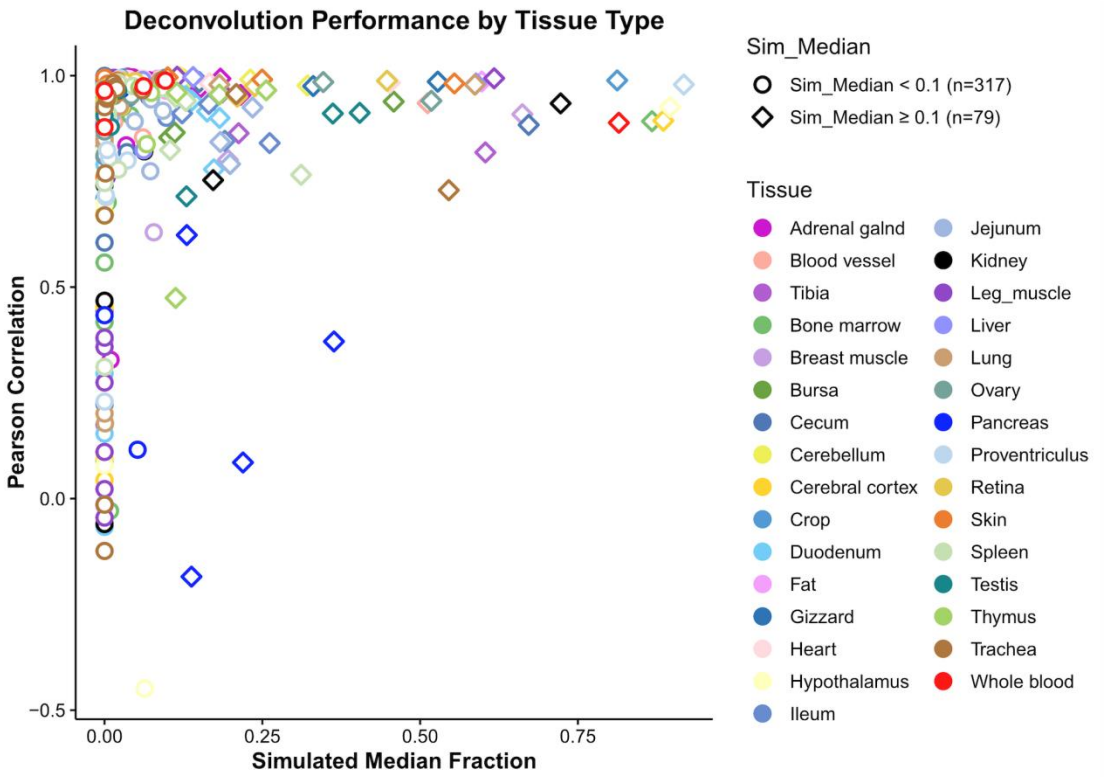

Supplementary Fig. 30. Correlation between median cell fraction and deconvolution accuracy

Scatter plot showing the relationship between median cell fraction and deconvolution accuracy for 127 cell types.

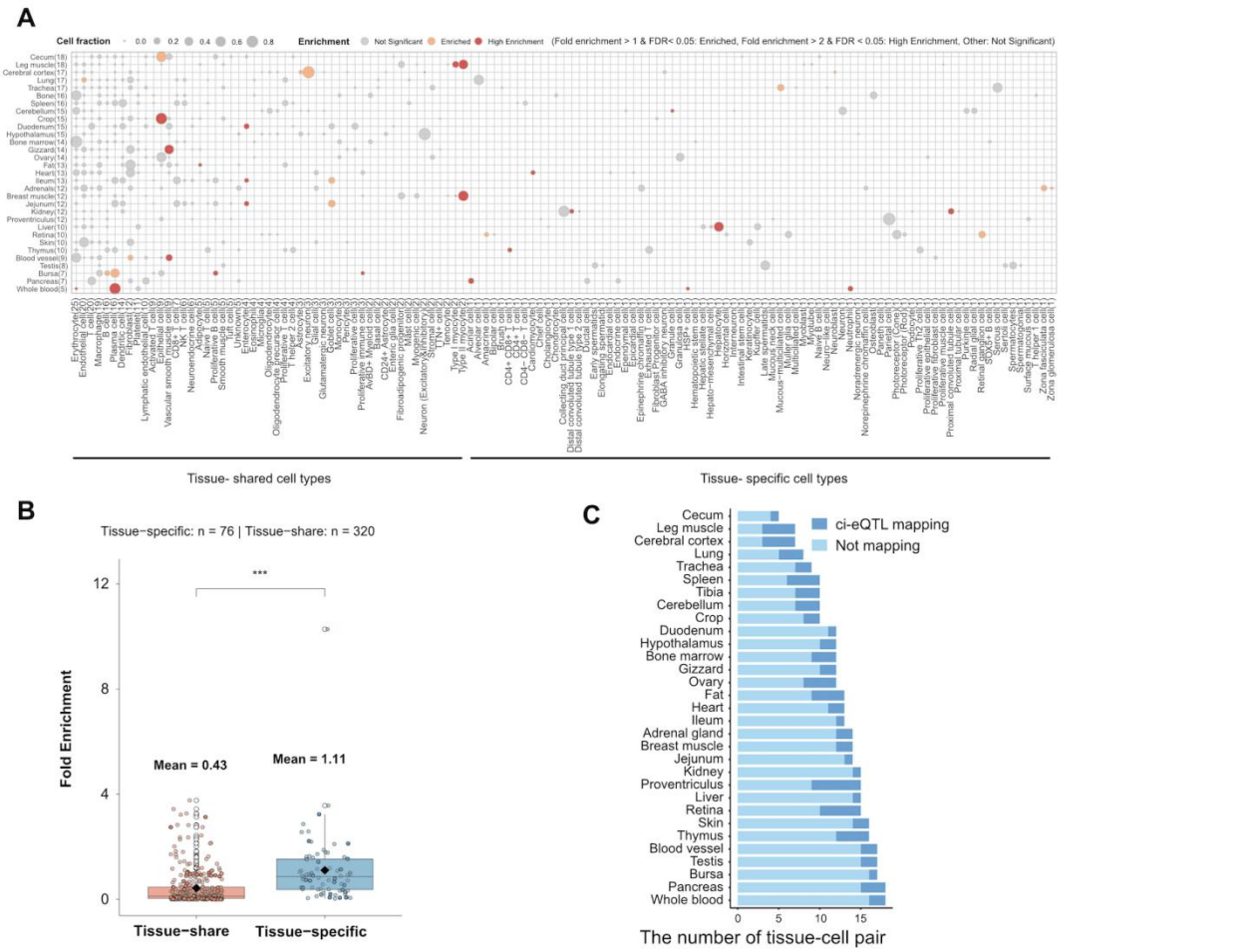

Supplementary Fig. 31. Enrichment analysis of tissue-specific genes and cell type marker genes

(A) Enrichment of tissue-specific genes and same-tissue cell type marker genes. Grey dots = non-significant enrichment; colored dots = significant enrichment. Cell types are ordered by tissue-shared versus tissue-specific classification. **(B)** Summary of tissue-specific gene enrichment by marker genes from tissue-specific versus tissue-shared cell types. **(C)** Number of tissue-cell type pair used for cieQTL mapping.

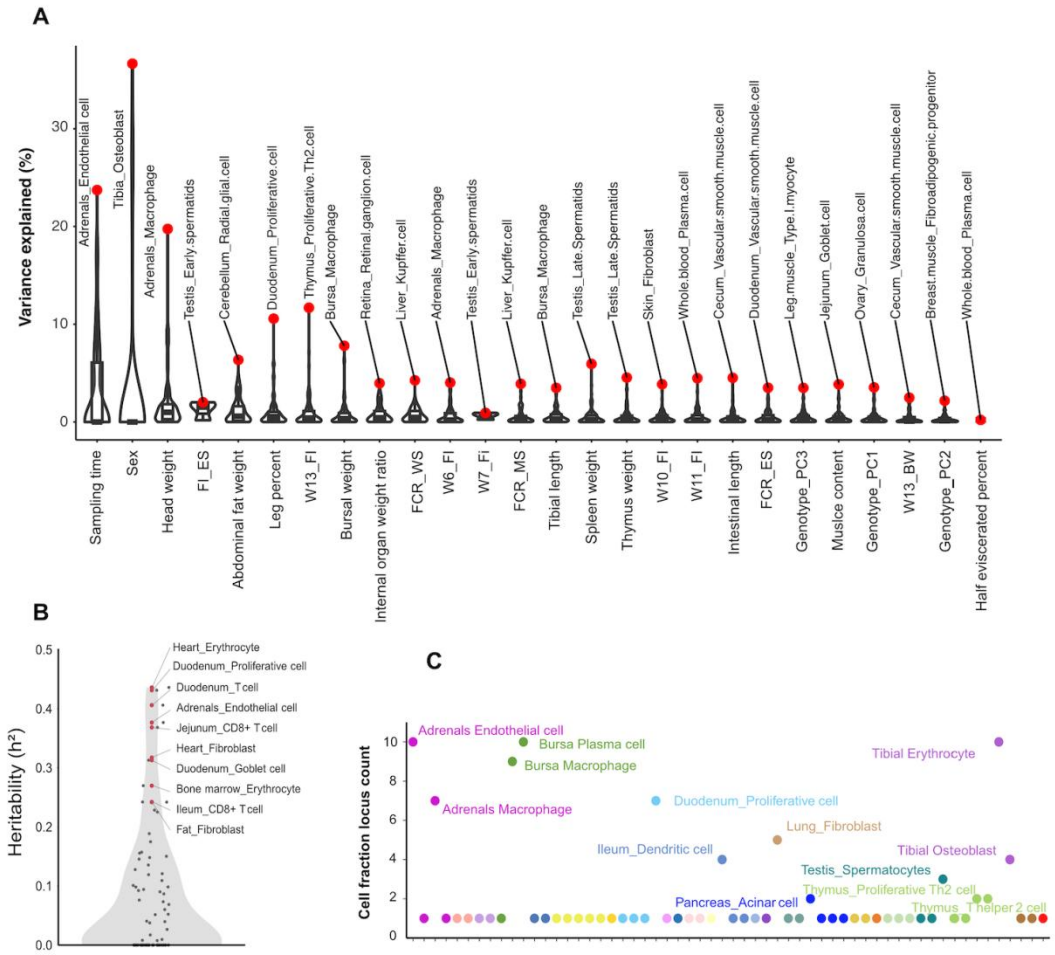

Supplementary Fig. 32. Characterization of factors influencing cell type proportions
(A) Variance analysis of 26 recorded metadata attributes explained by the cell type proportions, quantified using ANOVA. Red dots represent cell types explaining the highest variance for each metadata. **(B)** Heritability estimated for 79 cell type fractions from 280 ChickenSexGTEx cohort. **(C)** Summary of GWAS loci associated with 79 cell type fractions. Tissue types are color-coded as specified in Fig. 2E.

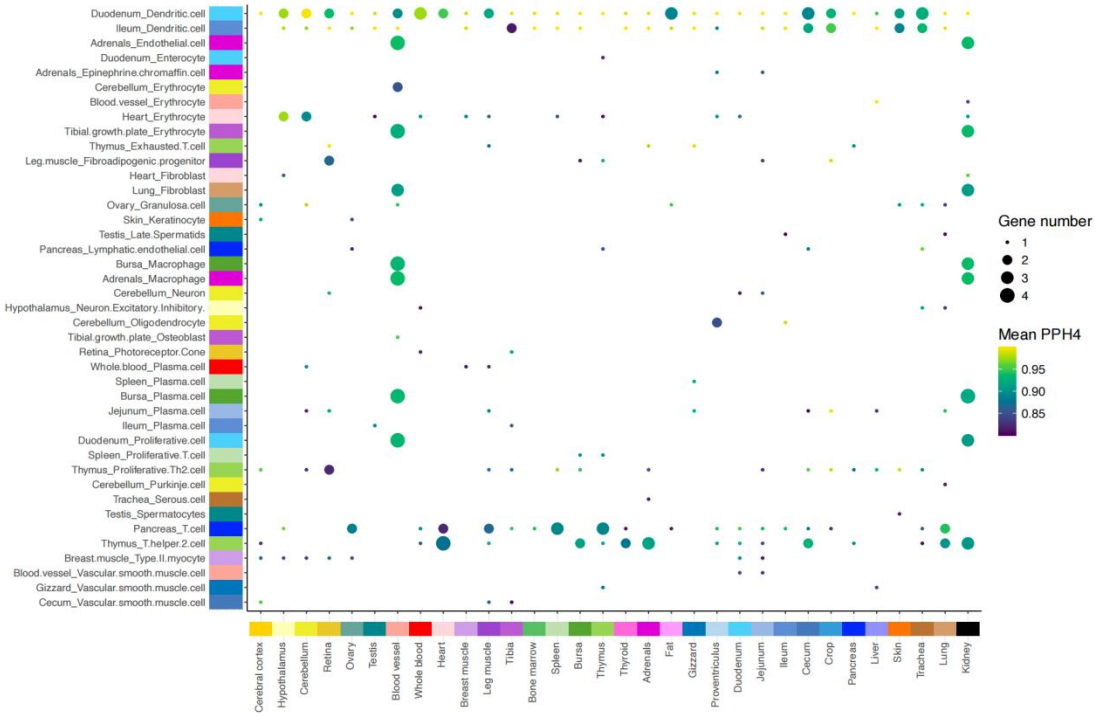

Supplementary Fig. 33. Colocalization of cell fraction cf-QTL with bulk tissue eQTL Rows represent GWAS loci associated with target cell fractions. Dots denote significant colocalization events (PP.H4 > 0.8). Dot size and darkness correspond to the number of colocalized genes and average PP.H4 value, respectively. Tissue types are color-coded as specified in Fig. 2E.

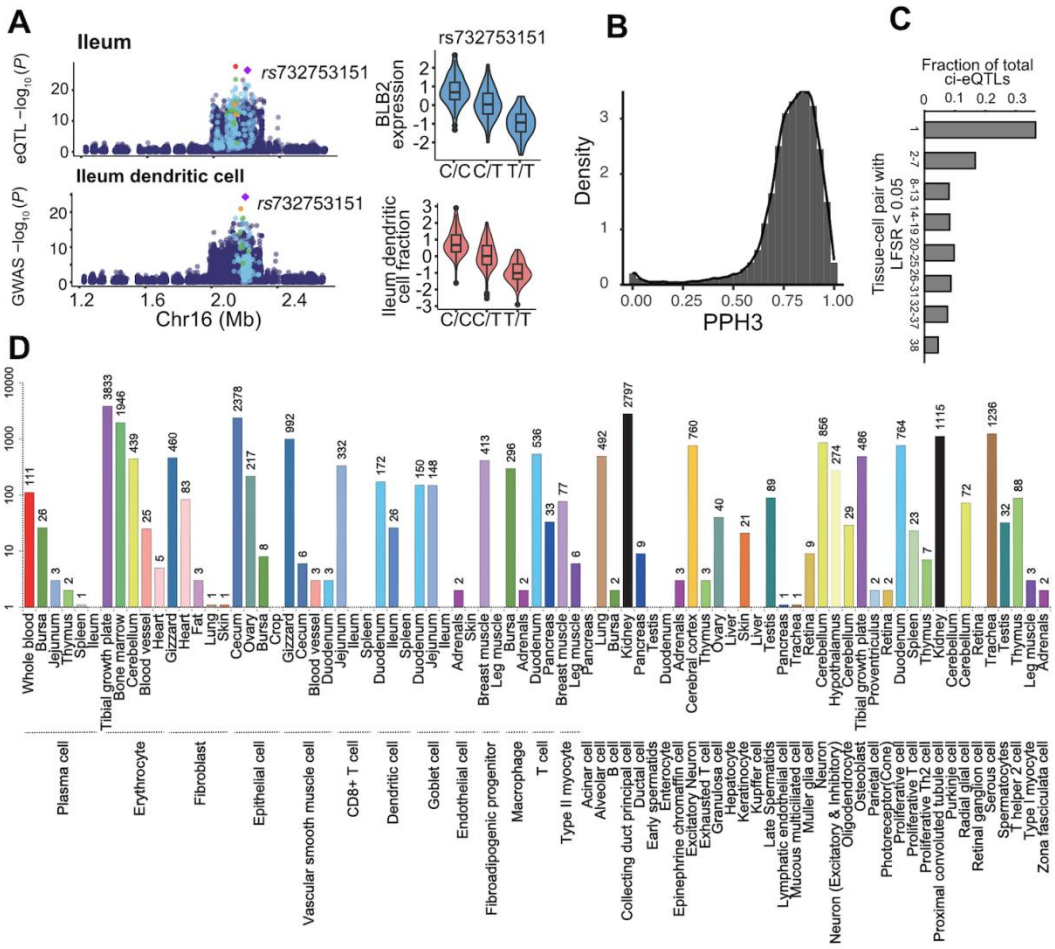

Supplementary Fig. 34. Cell-fraction interacted eQTL (cieQTL) mapping and characterization

(A) Representative example: a cfQTL (variant *rs732753151*) associated with ileum dendritic cell fractions, which colocalizes with an eQTL regulating *BLB2* expression in ileum. Right panel: boxplots of *BLB2* expression and ileum dendritic cell fractions stratified by *rs732753151* genotype. **(B)** Distribution of colocalization probabilities (PP.H3) between cieQTL and bulk tissue eQTL. **(C)** Fraction of cieQTL shared across varying numbers of tissue cell types (LFSR < 0.05). **(D)** Number of cieGenes detected across all tissue-cell type pairs. Tissue types are color-coded as specified in Fig. 2E.

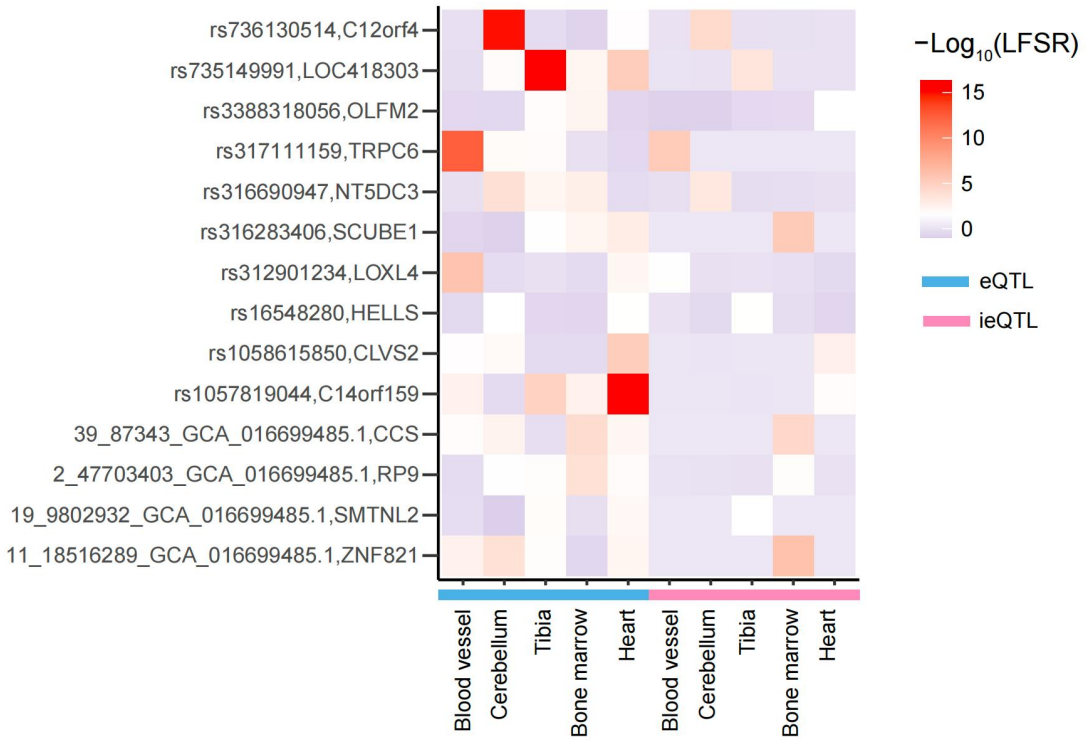

Supplementary Fig. 35. Comparative tissue-specificity of variant-mediated gene regulation in erythrocytes versus bulk tissues

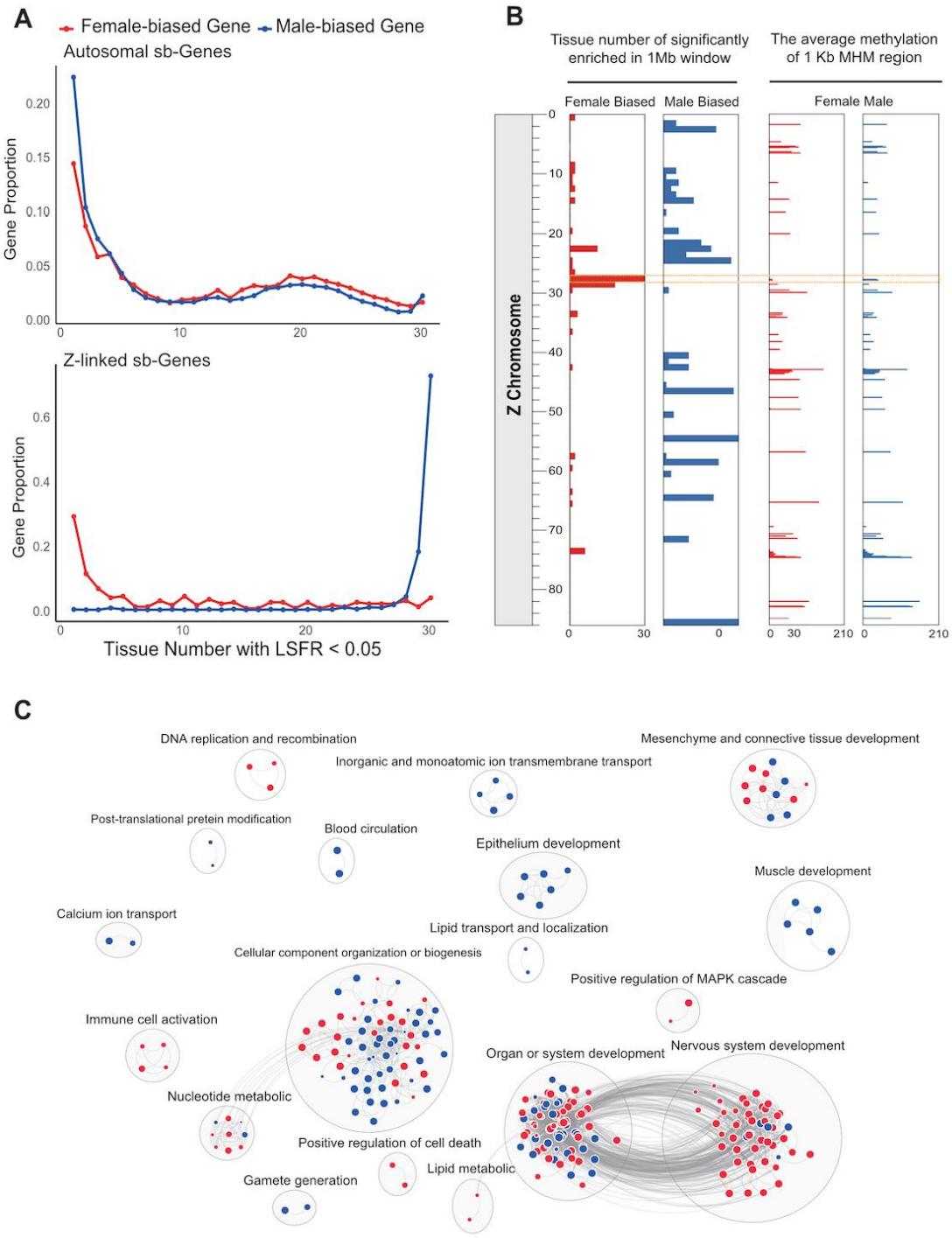

Supplementary Fig. 36. Functional annotation and tissue-sharing of sex-biased genes
(A) MashR-derived tissue-sharing patterns of male- and female-biased genes across 30 tissues. Top panel = autosomal sbGenes; bottom panel = Z-linked sbGenes. **(B)** Landscape of sex-biased enrichment and male-hypermethylated (MHM) region methylation across the Z chromosome. Left panels show, for each 1-Mb window along the Z chromosome (y-axis), the number of tissues in which the window is significantly enriched for female-biased (red) or male-biased (blue) genes (x-axis). Right panels display the average DNA methylation level within 1-kb

MHM region(s) for females (red) and males (blue). The orange lines highlight a 30-tissue-shared female-biased region overlapping with a previously reported MHM region. **(C)** Clusters of functionally related gene sets enriched for sex-biased expression across tissues. Balloons denote enriched gene sets (female-biased, red; male-biased, blue), with sizes proportional to the across-tissue GSEA meta-analysis significance. Edges connect gene sets sharing leading-edge genes.

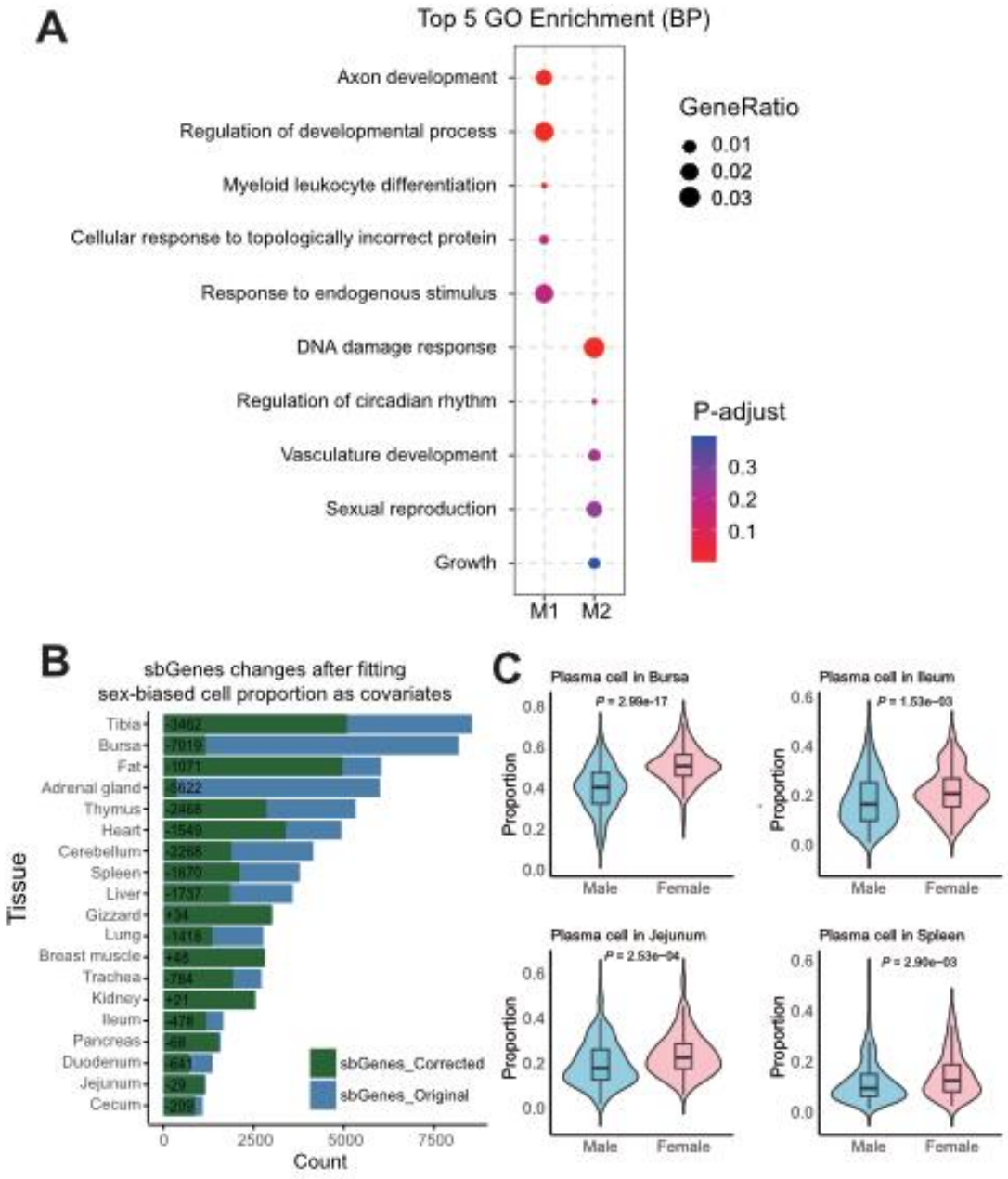

Supplementary Fig. 37. Characterization of sex-biased co-expression modules and cell types

(A) GO enrichment analysis of gene sets in sex-biased modules M1 and M2 identified in hypothalamus. **(B)** Identification of sex-biased genes following adjustment for sex-biased cell

type proportions as covariates, across 30 tissues. **(C)** Female-biased plasma cell proportions in bursa, ileum, jejunum, and spleen tissues, respectively.

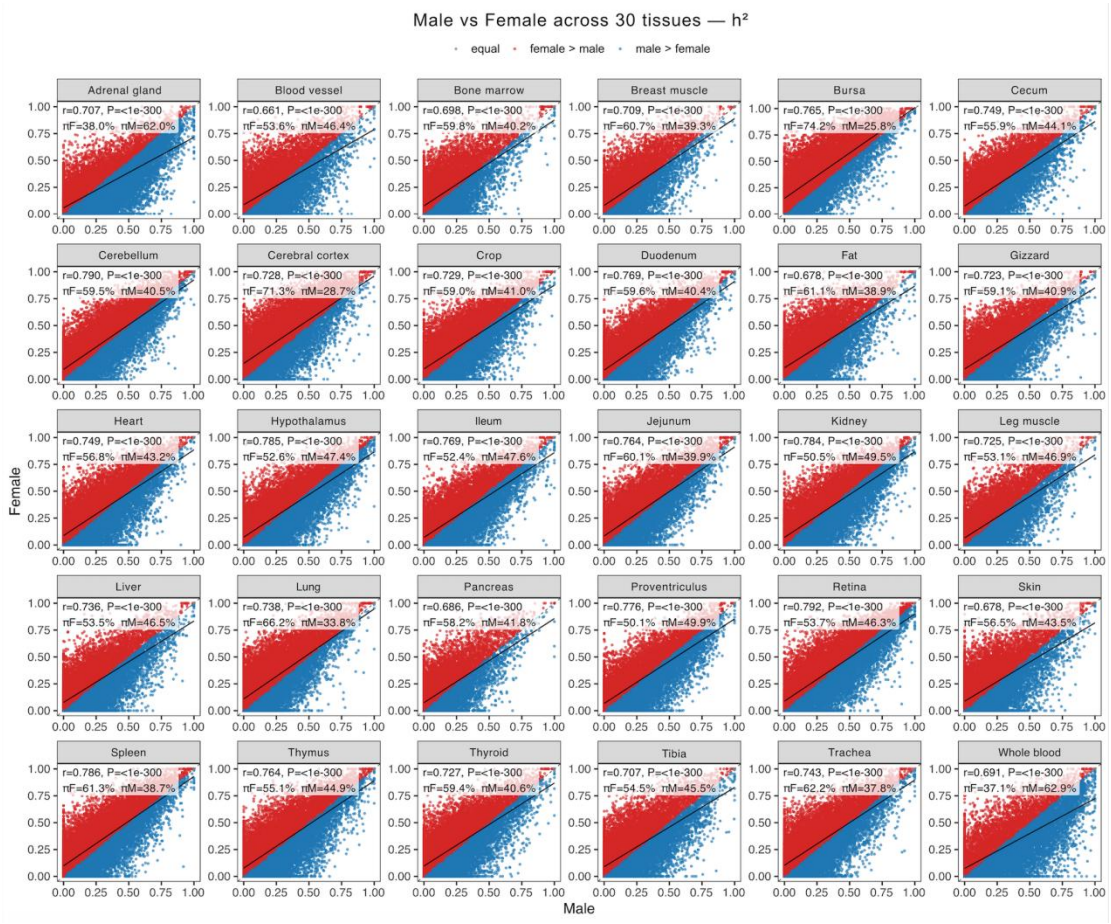

Supplementary Fig. 38. Correlations of *cis*-h^2 estimates for gene expression in male- and female-stratified populations

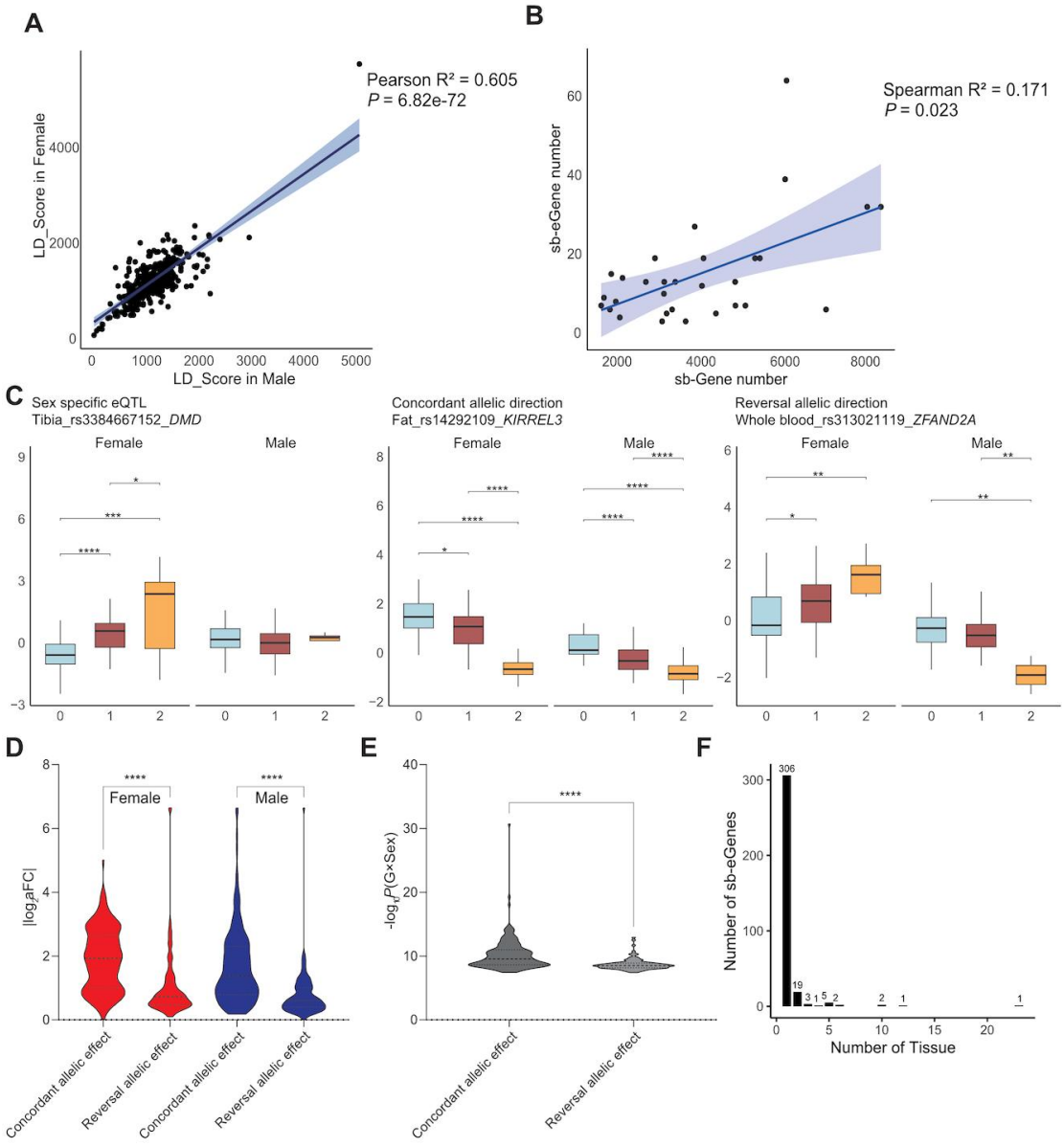

Supplementary Fig. 39. Sex-stratified population structure and sex-biased gene regulation **(A)** Correlation of LD scores calculated from male- and female-stratified subpopulations. **(B)** Correlation of sbGene number and sb-eGene number. **(C)** Examples of sex-specific (left), sex-different (middle), and sex-reversed eQTL (right). **(D)** Comparison of absolute effect sizes between sex-different and sex-reversed eQTL in male- and female-stratified subpopulations. **(E)** G×Sex interaction significance comparison between sex different and sex-reversed eQTL. **(F)** Distribution of tissue overlap for sb-eGenes.

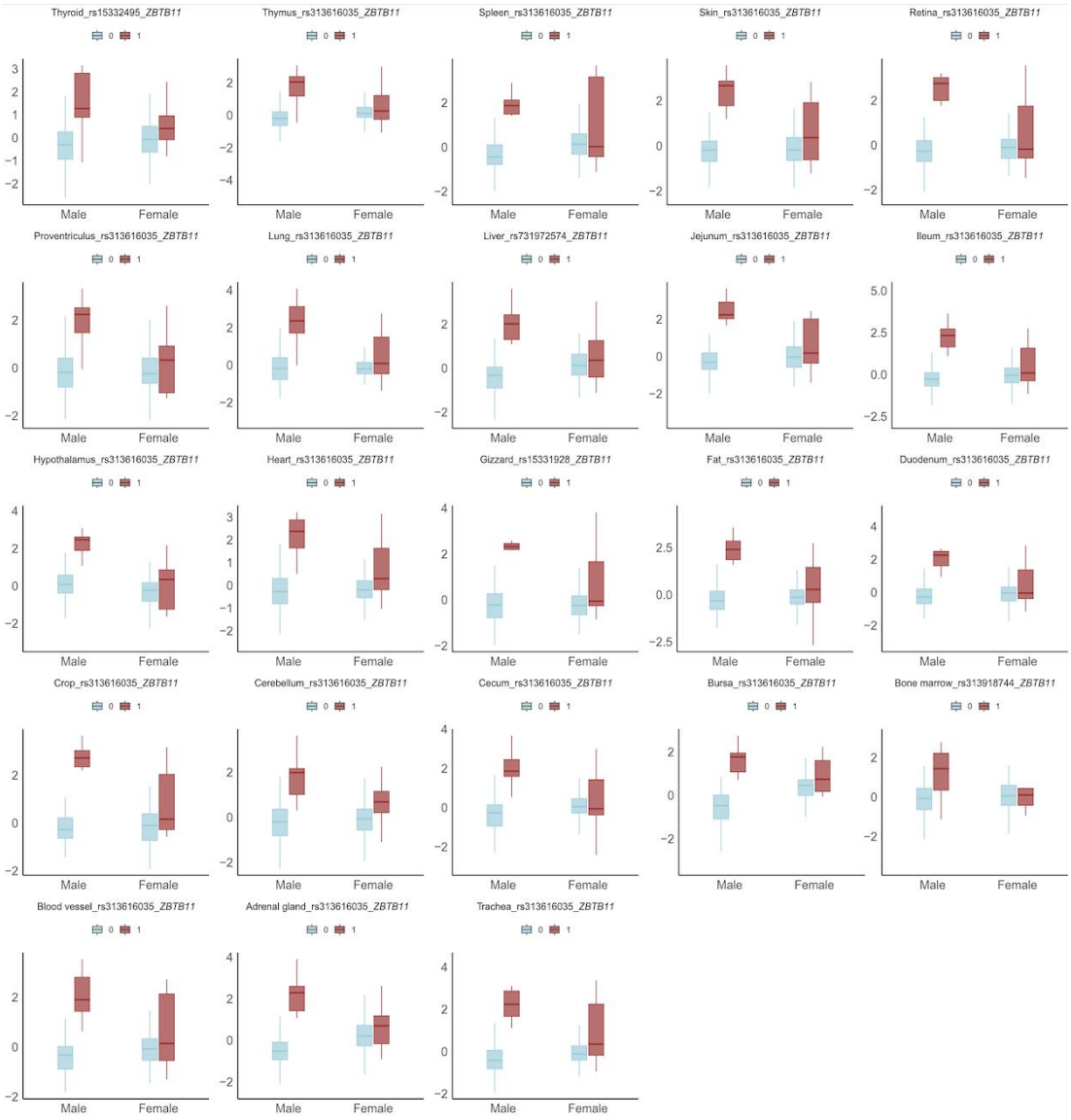

Supplementary Fig. 40. Example of the concordant effects of the male-biased eQTL rs15332495 in regulating *ZBTB11* across 23 tissues

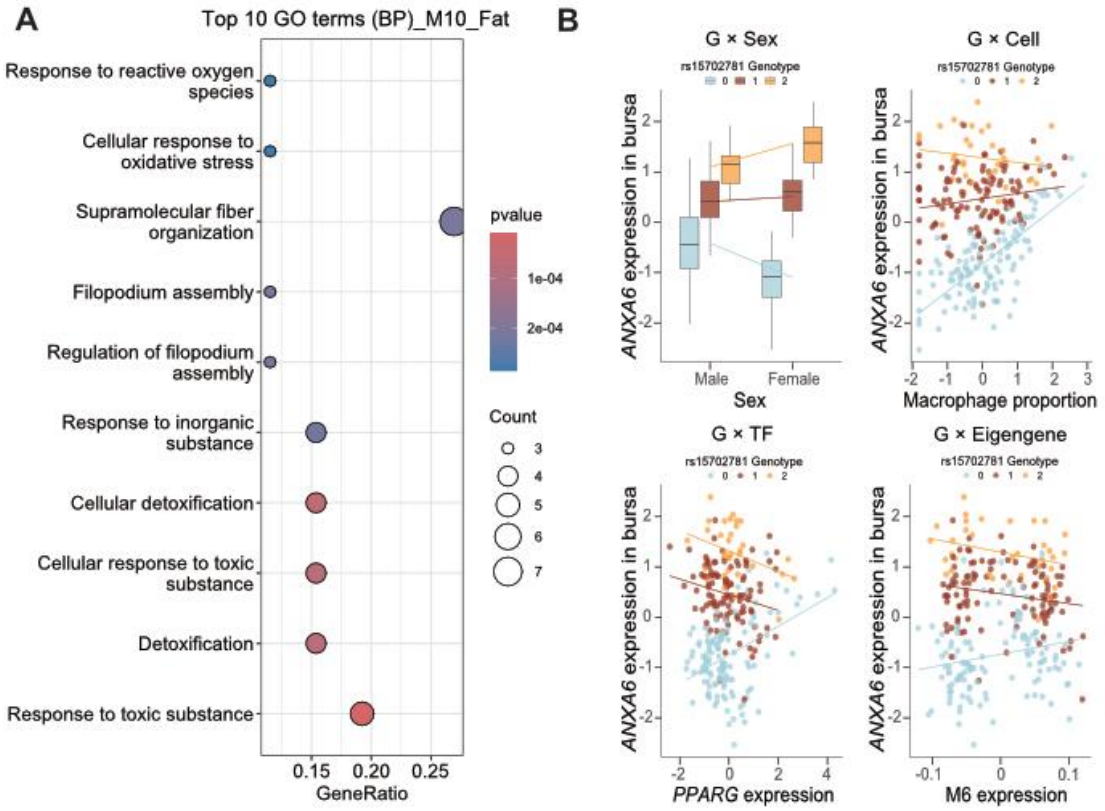

Supplementary Fig. 41. Mechanistic mediation analysis of sex-biased gene regulation **(A)** GO enrichment of gene sets in coexpression module M10 identified in fat tissue. **(B)** Example of the sex-biased eQTL *rs15702781* in regulating *ANXA6* expression, mediated by macrophage proportion, transcriptional factor *PPARG* gene expression, and eigengene expression of module M6 in bursa.

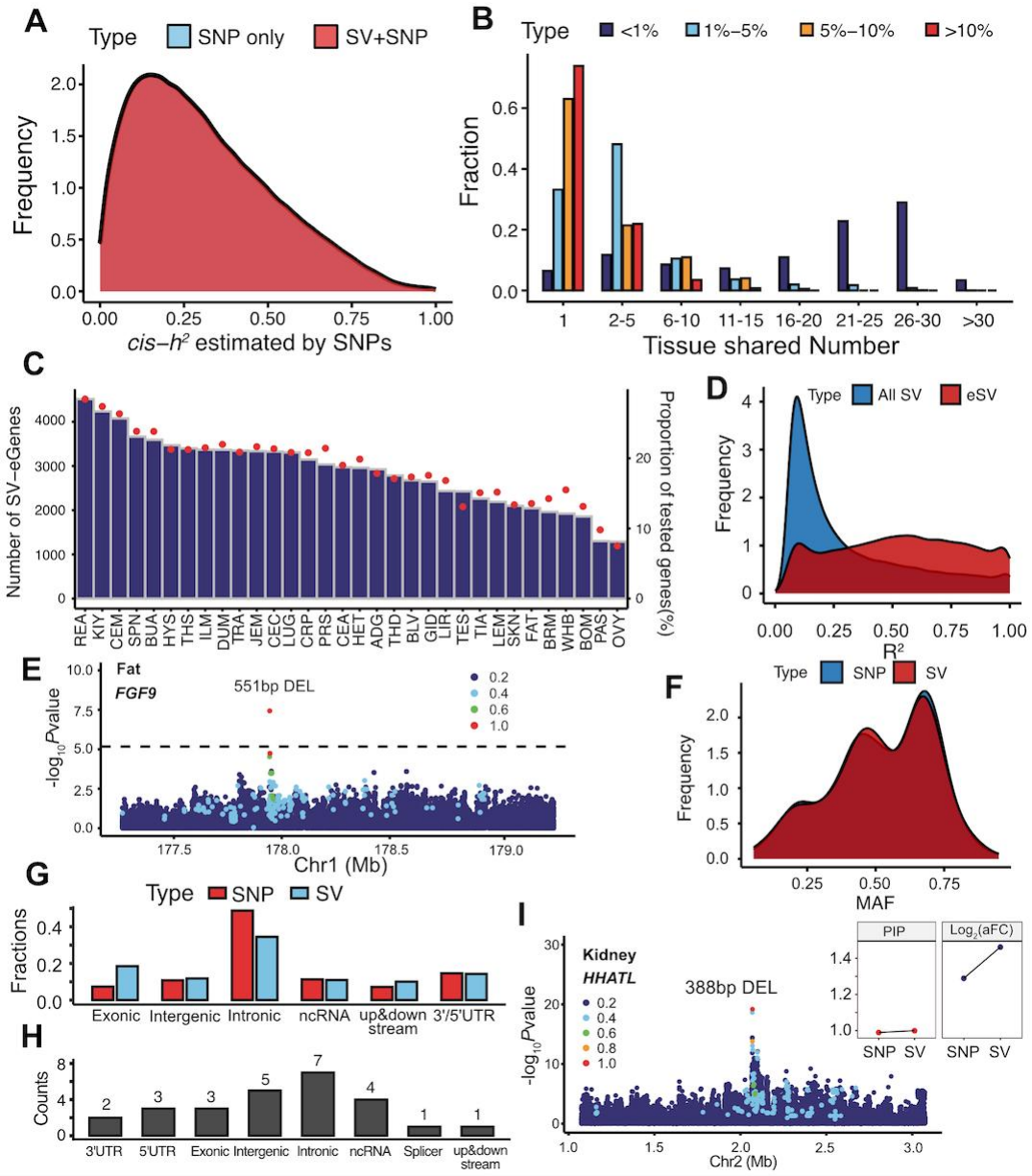

Supplementary Fig. 42. Estimation of *cis-h2* with SV inclusion and SV-mediated genetic regulation across tissues

(A) Distribution of gains in *cis-h*^{2} following the inclusion of SV in the estimation model. **(B)** Proportion of genes stratified by tissue-sharing number, categorized according to the magnitude of cis-h² increase conferred by SV inclusion. **(C)** Number of SV-eGenes detected and their proportion relative to all tested genes across 32 tissues. Bars represent the SV-eGene counts; points represent the proportion of SV-eGenes among tested genes. **(D)** Comparison of LD distribution between expression-associated (eSV), all SV, and SNP. **(E)** Example of *FGF9* expression regulated exclusively by SV but not by SNP in adipose tissue. **(F)** Distribution of MAF-matched fine-mapped SNP and SV that regulate the same gene expression. **(G)** Fractions of MAF-matched fine-mapped SV-eQTL and SNP-eQTL located within functional genomic regions. **(H)** Fractions of fine-mapped SV-leading eQTL distributed across functional genomic regions. **(I)** Example of a fine-mapped SV-leading eQTL regulating *HHATL* expression in

kidney, exhibiting high posterior inclusion probability (PIP) and effect size compared to SNP within the same fine-mapped credible set.

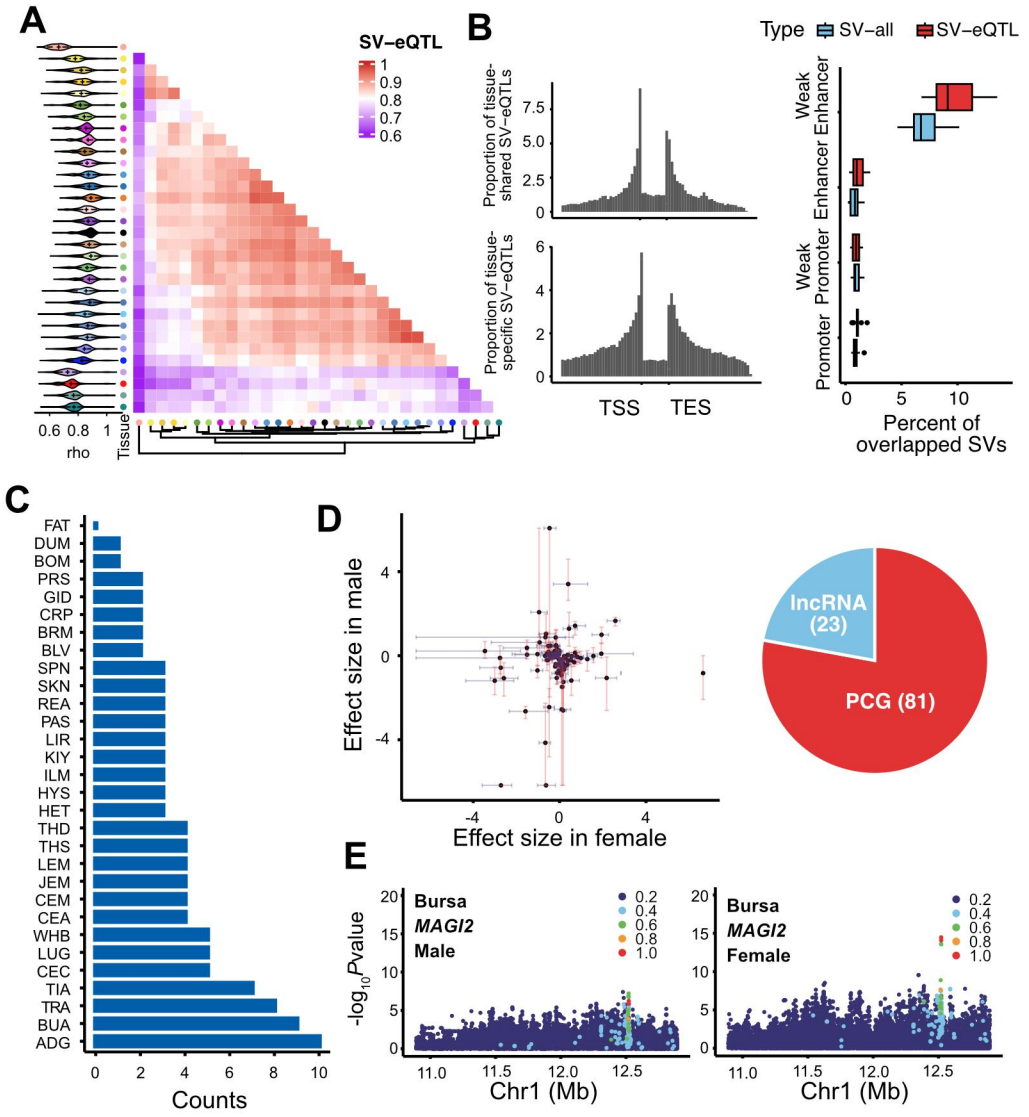

Supplementary Fig. 43. Tissue-sharing patterns and sex-biased regulation of SV-eQTL
(A) Pairwise tissue-sharing patterns of SV-eQTL effect sizes, shown as Spearman's correlation coefficients (left: distribution per tissue; bottom: hierarchical clustering of tissues by regulatory similarity). Tissue types are color-coded as in Fig. 2E. **(B)** Distance to TSS of tissue-shared (top) and tissue-specific (bottom) SV-eQTL, along with functional enrichment of SV-eQTL within annotated enhancer and promoter regions. **(C)** Counts of sex-biased SV-eQTL identified across 32 tissues. **(D)** Effect size estimates of sex-specific SV-eQTL in male- and female-stratified subpopulations. Points and bars represent mean effect sizes and confidence intervals. Sex-specific SV-eQTL are defined as loci whose confidence interval overlaps with zero in one sex but not the other. Right panel: pie chart showing the distribution of genes under sex-specific regulation. **(E)** Representative example of female-specific regulation of *MAGI2* regulation by a 596 bp insertion in bursa tissue.

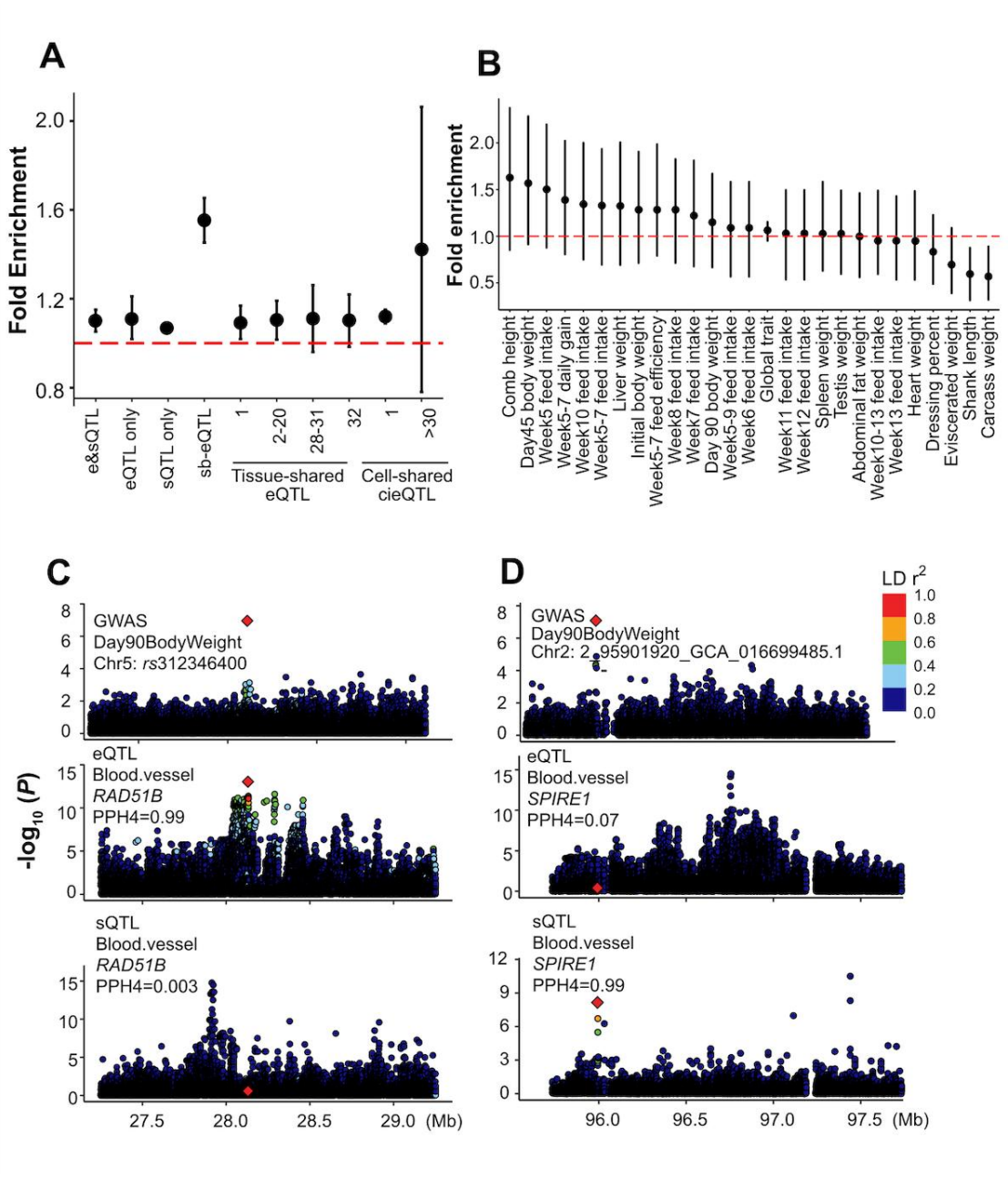

Supplementary Fig. 44. Genetic enrichment of molQTL and context-dependent QTL with complex traits, and examples of the specialized colocalization with molQTL
(A) Fold enrichment of complex trait GWAS loci with molQTL, sb-eQTL, tissue-specific or shared eQTL, cell type-specific or shared cieQTL. **(B)** Summary of fold enrichment results of sb-eQTL with different complex traits. **(C)** Colocalization of day 90 body weight GWAS locus (*rs312346400*) with eQTL only in regulating the expression of *RAD51B* in blood vessel. **(D)** Colocalization of day 90 body weight GWAS locus (*2_95901920_GCA_016699485.1*) with eQTL only in regulating the expression of *RAD51B* in blood vessel.

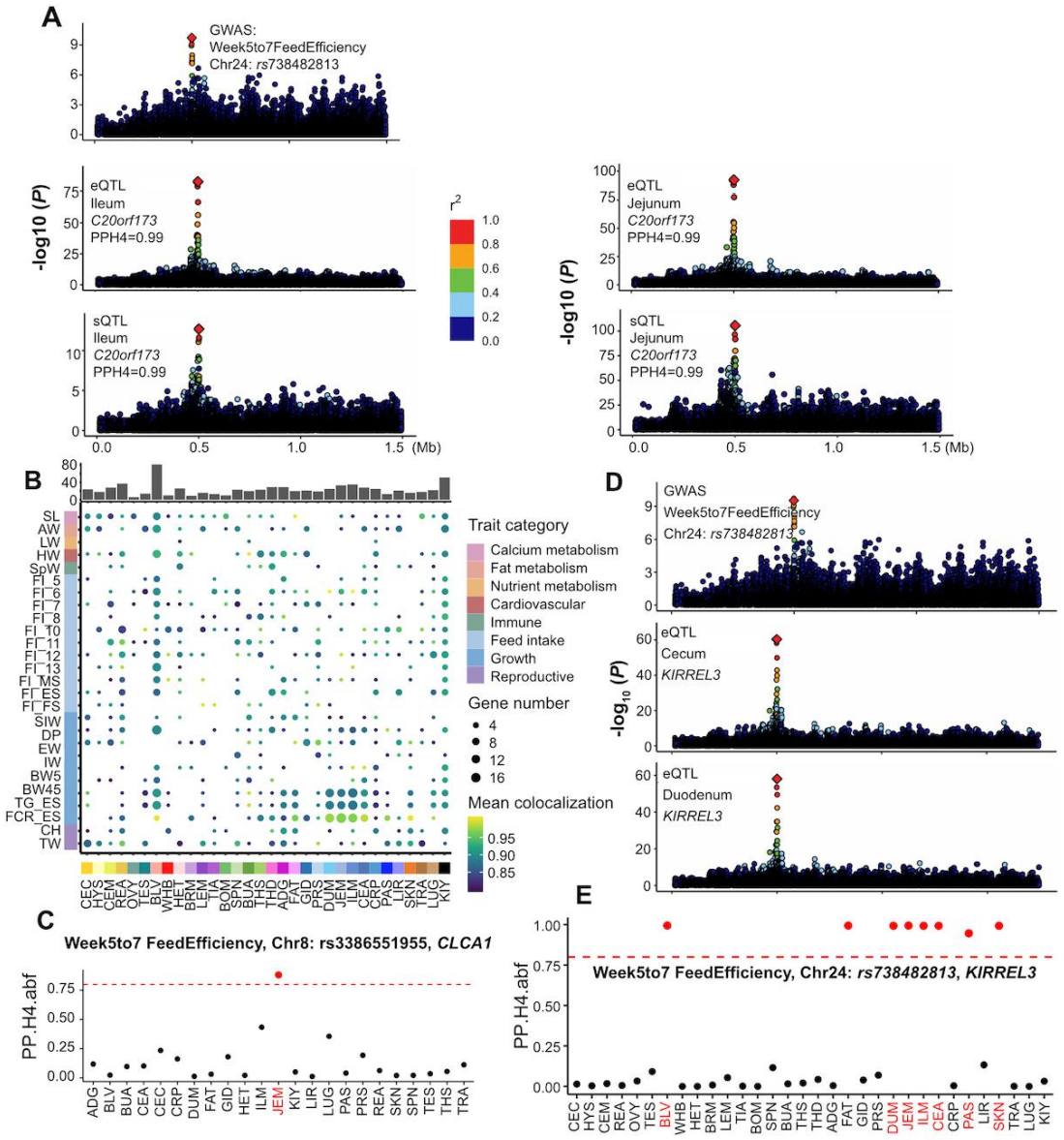

Supplementary Fig. 45. Examples and summary of complex trait GWAS loci colocalized with molQTL, content-dependent eQTL or tissue-specific eQTL.
(A) The colocalizations of week 5-7 feed efficiency GWAS signal *rs738482813* with both eQTL and sQTL of *C20orf173* in additional intestinal tissues except for cecum listed in Fig. 9B. **(B)** Summary of all significant colocalization signals (PP.H4 > 0.8) across all tissues and complex traits, which categorized into 8 groups. The top barplot showed the sum of total colocalized genes identified in each tissue. **(C)** Tissue-specific eQTL colocalization example. Week 5-7 GWAS locus *rs3386551955* shows to colocalize with the *CLCA1* eQTL exclusively in jejunum. The red dash line indicate the PP.H4 = 0.8. **(D)** Multi-tissue colocalization example of *KIRREL3* eQTL with week 5-7 feed efficiency GWAS signal (*rs738482813*). **(E)** *KIRREL3* eQTL multi-tissue colocalization example. Week 5-7 GWAS locus *rs738482813* shows to colocalize with the *KIRREL3* eQTL in blood vessel, duodenum, jejunum, ileum, cecum, pancreas, and skin. The red dash line indicate the PP.H4 = 0.8.

Supplementary Table 1: Summary of tissue type information and anatomical sites of samples collected from ChickenSexGTEx cohort.

Anatomical system	Tissue type	Abbreviations	Anatomical position	Sample size (Female, Male)
Cardiovascular	Blood vessel	BLV	Aortic arch, the major blood vessel from the left ventricle of the heart.	249 (116, 133)
	Heart	HET	Apex of the heart, the inferolateral region of the left ventricle.	273 (126, 147)
	Whole blood	WHB	Wing vein blood.	195 (100, 95)
Digestive	Crop	CRP	Mid-region of the crop, including mucosa, submucosa, muscularis externa, and serosa	272 (125, 147)
	Proventriculus	PRS	Mid-region of the proventriculus, including mucosa, submucosa, muscularis externa, and serosa.	274 (127, 147)
	Gizzard	GID	Mid-region of the muscular lateral part of gizzard with the cuticle removed.	275 (129, 146)
	Duodenum	DUM	Proximal duodenal mucosal layers, approximately 2-3 centimeters distal to the connection to gizzard.	274 (128, 146)
	Jejunum	JEM	Proximal jejunal mucosal layers, approximately 5-7 centimeters distal to the duodenojejunal flexure.	274 (127, 147)
	Ileum	ILM	Distal ileal mucosal layers, approximately 1-3 centimeters proximal to the ileocecal junction.	273 (129, 144)
	Cecum	CEA	Proximal region of the right cecal mucosal layers, approximately 3-4 centimeters to the blind-ended pouch.	275 (129, 146)
	Pancreas	PAS	Pancreatic body, mid-region of the pancreas.	267 (126, 141)

	Liver	LIR	Right lobe of the liver parenchyma, avoiding major blood vessels and bile ducts.	278 (130, 148)
Endocrine	Abdominal Fat	FAT	Central region of the abdominal fat pad, avoiding any adjacent muscle or visceral organs.	264 (120, 144)
	Adrenal gland	ADG	The whole paried adrenal gland, cranial to the kidney.	263 (124, 139)
	Thyroid	THD	The whole right thyroid gland, located adjacent to the right carotid artery and right jugular vein.	269 (127, 142)
Lymphatic	Bone marrow	BOM	Left tibia bone marrows, distributed in the medullary cavity of the tibia.	269 (127, 142)
	Bursa	BUA	Central region of the bursa, which is located dorsal to the cloaca.	277 (129, 148)
	Spleen	SPN	Mid-region of the spleen, near the proventriculus and gizzard.	274 (128, 146)
	Thymus	THS	One of the cranial lobes of the thymus, located in the cervical and thoracic regions.	260 (125, 135)
Motor	Tibial growth plate	TIA	Growth plate of the tibia, the hyaline cartilage located the proximal end of the tibia.	257 (119, 138)
	Breast muscle	BRM	Pectoralis major muscle, particularly selected from the mid-region of the pectoralis major.	267 (126, 141)
	Leg muscle	LEM	Mid-belly region of the gastrocnemius.	275 (127, 148)
Nervous	Cerebral cortex	CEC	Dorsal region of the right cerebral cortex.	271 (129, 142)
	Hypothalamus	HYS	The base of the diencephlon, right below the thalamus.	252 (122, 130)
	Cerebellum	CEM	Vermis (midline region) of the cerebellum.	271 (128, 143)

Reproductive	Ovary	OVY	Left ovary follicles and stroma, avoiding collecting the kidneys and adrenal glands.	127
	Testis	TES	Mid-region of the left testis, avoiding the epididymis.	146
Respiratory	Lung	LUG	Mid-region of the right lung, including the parabronchi, blood vessels and connective tissues.	276 (127, 149)
	Trachea	TRA	Mid-cervical region of trachea, mainly to include the cartilaginous rings and epithelium.	275 (126, 149)
Sensory	Retina	REA	Retina layers, located at the posterior part of the eyeball between the virteous humor and the choroid.	265(121, 144)
	Skin	SKN	Mideline region of the dorsal skin between the scapulae and the base of the tail, without feathers.	251 (123, 128)
Urinary	Kidney	KIY	Mid-part of the middle lobe of the kidney, avoiding adrenal gland or ureter.	275 (125, 150)

Supplementary Table 2: Comparison of identified eGenes and sGenes numbers between ChickenSexGTEx and ChickenGTEx pilot phase

Tissue	ChickenSexGTEx		ChickenGTEx pilot phase	Overlap	Type
	eGene/sGene	independent QTL			
Adrenal gland	12656	22449	0	0	eGene
Blood vessel	11052	16737	0	0	eGene
Bone marrow	9213	14257	0	0	eGene
Breast muscle	9062	14298	0	0	eGene
Bursa	12364	22874	1101	995	eGene
Cecum	12008	20692	184	140	eGene
Cerebellum	13369	22439	268	250	eGene
Cerebral cortex	12741	23803	0	0	eGene
Crop	11762	20460	0	0	eGene
Duodenum	12161	22022	18	12	eGene

Fat	9959	15683	1186	973	eGene
Gizzard	10805	18342	0	0	eGene
Heart	11304	20082	2271	1906	eGene
Hypothalamus	12383	22546	1307	1123	eGene
Ileum	12203	21826	21	17	eGene
Jejunum	12118	21721	78	64	eGene
Kidney	12799	23783	618	534	eGene
Leg muscle	9870	15893	0	0	eGene
Liver	10703	18003	8644	6352	eGene
Lung	12330	21681	50	44	eGene
Ovary	11085	15706	748	497	eGene
Pancreas	7990	11829	0	0	eGene
Proventriculus	11193	20887	0	0	eGene
Retina	13927	24250	1556	1486	eGene
Skin	10411	16382	838	617	eGene
Spleen	12601	22688	6597	5397	eGene
Testis	14268	23160	63	43	eGene
Thymus	12947	23486	307	290	eGene
Thyroid	12464	21895	0	0	eGene
Tibia	11096	18713	0	0	eGene
Trachea	12663	21817	1819	1651	eGene
Whole blood	9667	16746	4287	3119	eGene
Adrenal gland	5600	8885	0	0	sGene
Blood vessel	6285	9099	0	0	sGene
Bone marrow	4015	6047	0	0	sGene
Breast muscle	4284	6437	0	0	sGene
Bursa	5562	10372	436	301	sGene
Cecum	6014	10374	84	52	sGene
Cerebellum	5552	9345	80	50	sGene
Cerebral cortex	5209	8428	0	0	sGene
Crop	5182	8446	0	0	sGene
Duodenum	5641	10085	51	27	sGene
Fat	4366	6675	441	267	sGene
Gizzard	4996	8201	0	0	sGene
Heart	4932	7971	703	446	sGene
Hypothalamus	5443	8743	515	314	sGene
Ileum	6042	10806	194	116	sGene

Jejunum	5798	10241	152	113	sGene
Kidney	5911	10884	187	129	sGene
Leg muscle	4402	6789	0	0	sGene
Liver	4387	7012	4594	2225	sGene
Lung	6069	10426	284	187	sGene
Ovary	6166	9546	618	332	sGene
Pancreas	1885	2581	0	0	sGene
Proventriculus	3954	6403	0	0	sGene
Retina	5834	10027	233	162	sGene
Skin	4792	7247	362	190	sGene
Spleen	5804	10822	4294	2601	sGene
Testis	7626	13852	117	64	sGene
Thymus	5672	10191	110	69	sGene
Thyroid	5551	8951	0	0	sGene
Tibia	4907	7741	0	0	sGene
Trachea	5863	9760	393	278	sGene
Whole blood	3774	6808	2366	1112	sGene

Supplementary Table 3: Summary information of 26 complex traits and number of significant GWAS loci

Trait	Abbreviations	Sample_size	Number of GWAS signals with different significance threholds	
			P_val(0.00001)	P_val(0.00000005)
Adipose weight	AW	907	557	199
Comb Height	CH	743	165	0
Day45 Body Weight	BW45	1531	399	113
Day90 Body Weight	BW90	1528	351	12
Dressing Percentage	DP	972	607	236
Eviscerated Weight	EW	984	230	1
Heart Weight	HW	974	365	42
Initial Body Weight	IW	1530	185	0
Liver Weight	LW	962	258	12
Tibial Length	SL	968	486	119
Carcass Weight	SIW	983	223	2
Spleen Weight	SpW	976	182	2
Testis Weight	TW	345	235	2
Week10 Feed Intake	FI_10	1515	191	2

Week11 Feed Intake	FI_11	1526	273	21
Week12 Feed Intake	FI_12	1518	678	224
Week13 Feed Intake	FI_13	1486	695	349
Week10to13 Average Feed Intake	FI_MS	1526	613	196
Week5 Feed Intake	FI_5	1529	313	77
Week5to7 Average Daily Gain	TG_ES	1521	335	82
Week5to7 Feed Conversion Ratio	FCR_ES	1469	203	9
Week5to7 Total Feed Intake	FI_ES	1531	591	229
Week5to13 Total Feed Intake	FI_FS	1521	203	1
Week6 Feed Intake	FI_6	1518	565	193
Week7 Feed Intake	FI_7	1516	528	197
Week8 Feed Intake	FI_8	1511	400	97

Supplementary References

1 Guan, D. et al. Genetic regulation of gene expression across multiple tissues in chickens. *Nat. Genet.* **57**, 1298-1308 (2025).

2 Dietrich, A. et al. SimBu: bias-aware simulation of bulk RNA-seq data with variable cell-type composition. *Bioinformatics* **38**, ii141-ii147 (2022).